HHS Public Access

Author manuscript

Sci Signal. Author manuscript; available in PMC 2016 March 29.

Published in final edited form as:

Sci Signal. ; 8(388): ra77. doi:10.1126/scisignal.aaa5823.

Semaphorin 3D autocrine signaling mediates the metastatic role of annexin A2 in pancreatic cancer

Kelly Foley[1,2,3], **Agnieszka A. Rucki**[1,2,3], **Qian Xiao**[1,2], **Donger Zhou**[1,2], **Ashley Leubner**[1,2], **Guanglan Mo**[1,2,4], **Jennifer Kleponis**[1,2], **Annie A. Wu**[1,2], **Rajni Sharma**[5], **Qingguang Jiang**[6,*], **Robert A. Anders**[1,2,5], **Christine A. Iacobuzio-Donahue**[1,2,5,†], **Katherine A. Hajjar**[7], **Anirban Maitra**[1,2,5,‡], **Elizabeth M. Jaffee**[1,2,3,4,5], and **Lei Zheng**[1,2,3,4,§]

[1]Sidney Kimmel Comprehensive Cancer Center, Johns Hopkins University School of Medicine, Baltimore, MD 21287, USA.

[2]Department of Oncology, Johns Hopkins University School of Medicine, Baltimore, MD 21287, USA.

[3]Graduate Program in Cellular and Molecular Medicine, Johns Hopkins University School of Medicine, Baltimore, MD 21287, USA.

---

§Corresponding author. lzheng6@jhmi.edu.
*Present address: Department of Neurobiology, Harvard University School of Medicine, Boston, MA 02115, USA.
†Present address: Department of Pathology, Memorial Sloan Kettering Cancer Center, New York, NY 10065, USA.
‡Present address: Department of Pathology, University of Texas M.D. Anderson Cancer Center, Houston, TX 77030, USA.

SUPPLEMENTARY MATERIALS

www.sciencesignaling.org/cgi/content/full/8/388/ra77/DC1

Fig. S1. AnxA2 staining in normal pancreas tissue, PanINs, and PDA from *KRAS*^{G12D} *TP53*^{R172H} *PDX-1-CRE*$^{+/+}$ mice.
Fig. S2. Histological characterization of PDAs from KPC and KPCA$^{-/-}$ mice.
Fig. S3. KPCA$^{-/-}$ cells have defects in lung metastasis formation in an IVC model of lung metastasis.
Fig. S4. Sema3A localization is unaffected by *ANXA2* expression.
Fig. S5. Knockdown of *ANXA2* in KPC cells results in decreased Sema3D secretion.
Fig. S6. The secretion of Sema3D is mediated by exocytosis and is partially regulated by Tyr^{23} phosphorylation of AnxA2.
Fig. S7. Sema3D binds to PlxnD1.
Fig. S8. Sema3D binds to NP-1 in KPC cells.
Fig. S9. Knockdown of *SEMA3D* expression or overexpression of *SEMA3D* does not alter cell proliferation or the rate of tumor growth.
Fig. S10. TGF-β is unable to induce nuclear localization of Snail-1 in *SEMA3D* knockdown PDA cells.
Fig. S11. Knockdown of *SEMA3D* does not alter primary tumor growth.
Fig. S12. Knockdown of *SEMA3D* does not alter primary tumor growth.
Fig. S13. Knockdown of *PLXND1* decreases invasion and metastasis of PDA cells.
Fig. S14. Exogenously overexpressed *SEMA3D* can be secreted from *ANXA2*-deficient PDA cells.
Fig. S15. Exogenous addition of Sema3D-AP to the culture medium partially restores the *ANXA2* siRNA–suppressed invasion capacity of Panc02 cells in a PlxnD1-dependent manner.
Fig. S16. Liver metastases can be visualized by ultrasound.
Fig. S17. Liver micrometastases are detectable by H&E analysis of liver sections.
Table S1. Primary tumor development was compared between mice expressing *ANXA2* (KPC) and mice lacking *ANXA2* expression (KPCA$^{-/-}$).

Author contributions: K.F., A.A.R., Q.X., D.Z., A.L., G.M., J.K., A.A.W., and R.S. performed experiments; K.F., A.A.R., Q.X., D.Z., A.M., E.M.J., and L.Z. analyzed the results; K.F. and L.Z. designed the experiments; R.A.A., C.A.I.-D., and A.M. performed the pathology analysis; Q.J. and K.A.H. provided critical materials; Q.J. and A.M. provided technical consultations; E.M.J. and L.Z. supervised all of the research; L.Z. conceived the project; K.F., E.M.J., and L.Z. wrote the manuscript.

Competing interests: E.M.J. and L.Z. hold a patent on annexin A2 as a target for cancer therapy. L.Z. has a pending patent on annexin A2 as an immunological target (U.S. Patent Application No. 14/249,534).

Data and materials availability: All microarray data used in this manuscript are deposited in Gene Expression Omnibus (www.ncbi.nlm.nih.gov/geo/) under GEO accession number GSE62285.

[4]Skip Viragh Center for Pancreatic Cancer, Johns Hopkins University School of Medicine, Baltimore, MD 21287, USA.

[5]Department of Pathology, Johns Hopkins University School of Medicine, Baltimore, MD 21287, USA.

[6]Department of Neuroscience, Johns Hopkins University School of Medicine, Baltimore, MD 21287, USA.

[7]Department of Pediatrics, Weill Cornell Medical College, New York, NY 10065, USA.

Abstract

Most patients with pancreatic ductal adenocarcinoma (PDA) present with metastatic disease at the time of diagnosis or will recur with metastases after surgical treatment. Semaphorin–plexin signaling mediates the migration of neuronal axons during development and of blood vessels during angiogenesis. The expression of the gene encoding semaphorin 3D (Sema3D) is increased in PDA tumors, and the presence of antibodies against the pleiotropic protein annexin A2 (AnxA2) in the sera of some patients after surgical resection of PDA is associated with longer recurrence-free survival. By knocking out *AnxA2* in a transgenic mouse model of PDA (KPC) that recapitulates the progression of human PDA from premalignancy to metastatic disease, we found that AnxA2 promoted metastases in vivo. The expression of *AnxA2* promoted the secretion of Sema3D from PDA cells, which coimmunoprecipitated with the co-receptor plexin D1 (PlxnD1) on PDA cells. Mouse PDA cells in which SEMA3D was knocked down or *ANXA2*-null PDA cells exhibited decreased invasive and metastatic potential in culture and in mice. However, restoring Sema3D in *AnxA2*-null cells did not entirely rescue metastatic behavior in culture and in vivo, suggesting that AnxA2 mediates additional prometastatic mechanisms. Patients with primary PDA tumors that have abundant Sema3D have widely metastatic disease and decreased survival compared to patients with tumors that have relatively low Sema3D abundance. Thus, AnxA2 and Sema3D may be new therapeutic targets and prognostic markers of metastatic PDA.

INTRODUCTION

Pancreatic ductal adenocarcinoma (PDA), a devastating malignant disease with a 5-year survival of less than 5%, is highly metastatic and resistant to most conventional chemotherapeutics (1). Surgical resection remains the primary treatment for PDA, but only 20% of patients present with locally resectable disease at the time of diagnosis, and most patients develop drug-resistant metastatic disease after surgical resection (2).

We recently identified the antibodies against a metastasis-associated protein, annexin A2 (AnxA2), in the sera of patients who were treated in a phase 2 study with an allogeneic, granulocyte-macrophage colony-stimulating factor (GM-CSF)–secreting tumor vaccine and who demonstrated prolonged recurrence-free survival after surgical resection of primary PDAs (3). In another study, the phosphorylation of Tyr^{23} in AnxA2 promoted metastases of PDA cells, whereas short hairpin RNA (shRNA)–mediated knockdown or antibody-mediated blockade of AnxA2 suppressed metastases in two murine transplantable tumor models (4).

Human PDA genome studies uncovered genetically altered molecular pathways that may regulate the metastatic process (5, 6). Although originally identified and characterized as axon guidance genes, genes encoding semaphorins and their cognate receptors (complexes composed of plexins and neuropilins) were found to be among the cellular pathways that are most frequently altered at the genetic level in PDA (5). The genes encoding axon guidance molecules, including class 3 semaphorins and plexins, were amplified in 18% of PDAs, and an additional 3% of PDAs had mutations in these genes. Previously, amplification of the gene encoding SEMA3A and the gene encoding a member of its receptor plexin A1 (PlxnA1) correlated with poor survival in PDA patients (7). Biankin *et al*. (5) found that the abundance of multiple semaphorins increased progressively during pancreatic tumorigenesis in a mouse model of PDA, further suggesting that dysregulation of these molecules contributes to PDA progression.

In addition to their known correlation with PDA survival, plexins also play a role in the development and progression of other cancer types. Specifically, PlxnD1 abundance is associated with high-grade primary and metastatic melanomas (8) as well as poorly differentiated cervical carcinoma tissues (9). By serving as a cellular receptor and signaling transducer for the class 3 semaphorin Sema3E, PlxnD1 promotes cancer cell invasiveness in multiple human tumor types and metastatic spreading in mouse models (10). In addition, Sema3E-PlxnD1 signaling suppresses apoptosis in metastatic breast cancer cells (11). These outcomes of increased PlxnD1 signaling are similar to those implicated for AnxA2 in PDA development (4). Like these axon guidance pathways, Semaphorin 3D (Sema3D) via PlxnD1 has been implicated in angiogenesis, invasion, cancer cell growth, and survival (12). Additionally, Sema3D and PlxnD1 have been shown to promote metastasis in various types of cancer and regulate the epithelial to mesenchymal transition (EMT) (13–15). Here, we investigated the mechanisms through which Sema3D-PlxnD1 signaling functions in PDA development and metastasis formation.

RESULTS

ANXA2 is essential for PDA metastasis formation in a transgenic mouse model of PDA

To evaluate the mechanism by which AnxA2 facilitates PDA development and metastases, we crossed *KRAS*^{G12D} *TP53*^{R172H} *PDX-1-CRE*$^{+/+}$ (KPC) mice, which are genetically engineered to develop spontaneous PDA tumors (16), and *ANXA2* homozygous knockout (*ANXA2*$^{-/-}$) mice to generate *KPCxANXA2*$^{-/-}$ (KPCA$^{-/-}$) mice. *ANXA2*$^{-/-}$ mice have a normal life span and fertility but display defects in neoangiogenesis in vivo and in ex vivo assays (17, 18). PDA development in the KPC mice recapitulates the progression from low-grade pancreatic intraepithelial neoplasms (PanINs) to invasive PDA in humans (16). We previously reported that the abundance of AnxA2 during the course of PDA development in KPC mice and in humans also increases with PanIN progression (4). AnxA2 is localized mainly in the cytoplasm of normal pancreatic epithelial cells and in the inner luminal surface of early PanIN lesions. However, this polarity of AnxA2 distribution is changed in later-stage PanINs when AnxA2 is relocated to the outer luminal surface in PanIN2 and PanIN3 lesions. In accordance with this, we found AnxA2 on the surface of all PanIN3 and invasive PDA cells (fig. S1).

Histological analysis confirmed the presence of primary PDAs in both cohorts of mice (Fig. 1A). Both KPC and KPCA$^{-/-}$ mice developed PanIN1 lesions at as early as 4 weeks of age. Additionally, both cohorts of mice developed PanIN2 and PanIN3 lesions at as early as 8 and 10 weeks of age, respectively. By 3 months of age, roughly 75% of mice in both cohorts had PanIN3 lesions, and by 4 months, an average of 65% of mice in both cohorts had histologically confirmed PDA when the mice were euthanized (table S1). In addition, primary tumors derived from KPC and KPCA$^{-/-}$ mice demonstrated similar rates of proliferation and apoptosis (fig. S2A). All KPC and KPCA$^{-/-}$ mice eventually died from the growth of primary PDA as previously observed with KPC mice (16); thus, there was also no observable difference in survival. However, despite these similarities in primary tumor growth between the KPC and KPCA$^{-/-}$ mice, the metastatic potential of PDA tumors differed between the two cohorts of mice: Upon gross examination of the mice in both cohorts, metastatic lesions were observed in the liver, peritoneal cavity, and lungs of 16 of 17 KPC mice (Fig. 1, B and C), whereas no observable gross metastatic lesions were seen in 23 KPCA$^{-/-}$ mice (Fig. 1, B and D). Despite the ability of primary PDA tumors to grow relatively close to the liver in KPCA$^{-/-}$ mice, only primary PDA tumors expressing *ANXA2* in KPC mice were able to invade and grow into the liver (Fig. 1E).

Because the function of AnxA2 in angiogenesis may play a role in controlling metastatic formation, we examined the vascular network in PDAs from KPC and KPCA$^{-/-}$ mice. We did not observe any obvious differences in the tumor vascular networks between KPC and KPCA$^{-/-}$ mice, as characterized by immunohistochemistry of the endothelial cell marker CD31 (fig. S2B) and the pericyte marker NG2 (fig. S2C), suggesting that the function of AnxA2 in angiogenesis is unlikely to mediate its role in PDA metastasis.

Reintroduction of ANXA2 restores the metastatic potential of ANXA2$^{-/-}$ PDA cells

Next, we investigated whether it was specifically the *ANXA2* deficiency or additional genetic alterations that led to the loss of metastatic potential in the PDA cells in KPCA$^{-/-}$ mice. To address this question, cell lines were established from the primary tumors of KPC and KPCA$^{-/-}$ mice to be used in a previously reported liver metastasis model in which cells were injected into the circulation via the spleen (4, 19). Western blot analysis confirmed that the cell line established from a KPCA$^{-/-}$ mouse had no detectable AnxA2 abundance, whereas the cell line established from a KPC mouse did (Fig. 2A). The KPC and KPCA$^{-/-}$ cell lines were then injected into the hemi-spleens of syngeneic mice, which were assessed for survival and liver colonization, over the course of, at most, 90 days. Most (8 of 10) of the mice that received an injection of KPCA$^{-/-}$ cells survived to the end of the 90-day study (two mice died as a result of tumors that formed at the splenic injection site) and none developed liver nodules (Fig. 2, B and C). In contrast, all mice that received an injection of KPC cells developed liver nodules and, accordingly, had relatively decreased survival (Fig. 2, B and C). In addition, we found that KPCA$^{-/-}$ cells were rarely able to form micrometastases and did not form colonies in the lung (fig. S3, A and B).

Because the above experiment showed that KPCA$^{-/-}$ cells injected into the hemi-spleen of syngeneic mice were unable to colonize the liver, we next investigated whether the restoration of *ANXA2* expression would enable KPCA$^{-/-}$ cells to colonize the liver. Full-

length *ANXA2* complementary DNA (cDNA) was introduced into KPCA$^{-/-}$ cells in culture by infection with a green fluorescent protein (GFP)–encoding lentivirus, and the cells were sorted by GFP expression. Although the expression amounts achieved were only ~25% of the endogenous amounts of AnxA2 in KPC cells (Fig. 2D), the transduced cells were able to colonize the liver and cause decreased survival in all mice that received a splenic injection of AnxA2-restored KPCA$^{-/-}$ cells (Fig. 2, E and F). Thus, AnxA2 has a major role in metastatic PDA colonization in this mouse model.

The expression of SEMA3D and PLXND1 is differentially regulated in pancreatic tumors from KPC versus KPCA$^{-/-}$ mice

We next used the KPC and KPCA$^{-/-}$ cell lines to investigate the downstream pathways that mediate the function of AnxA2 in PDA metastasis formation. A comprehensive mRNA expression profile comparing KPC and KPCA$^{-/-}$ cells using microarray gene expression analysis followed by Spotfire Gene Ontology Browser analysis revealed the top four gene functional categories that were enriched with genes of increased abundance and the top five gene functional categories that were enriched with genes of decreased abundance (Table 1). We prioritized in our studies the two functional categories (cell movement pathway and cell morphology and remodeling pathway) that were the most significantly enriched with genes of increased abundance and decreased abundance, respectively, because of their involvement in invasion and metastasis. We then chose the six genes that were the most significantly increased or decreased in abundance from each of the two functional categories for further validation (Fig. 3A).

To validate the differential expression of these 12 selected genes in PDA, their expression was analyzed in additional pancreatic tumors obtained from KPC and KPCA$^{-/-}$ mice by quantitative real-time reverse transcription polymerase chain reaction (qRT-PCR). The mRNA expression differences between the KPC and KPCA$^{-/-}$ tumors were largely consistent with the microarray analysis of the cell lines (Fig. 3B). *SEMA3D* and *PLXND1* were of particular interest because they both belong to gene families that are frequently amplified and mutated in human PDA (5). In addition, both genes were decreased in abundance in the absence of *ANXA2* (Fig. 3B), and both the class 3 semaphorin and plexin protein families were previously shown to have a ligand-receptor relationship. As shown in the Western blot analysis, the protein abundance of Sema3D was decreased in KPCA$^{-/-}$ cells compared to that in KPC cells, in accordance with the qRT-PCR results. However, the protein abundance of PlxnD1 was similar in both KPC and KPCA$^{-/-}$ cells (Fig. 3C).

Sema3D is aberrantly localized in PDA from KPCA$^{-/-}$ mice

Next, we examined the cellular localization of Sema3D and PlxnD1 by immunofluorescence staining. Immunofluorescence staining of pancreatic tissue from KPC mice demonstrated that both Sema3D and PlxnD1 were less detectable in normal pancreatic tissues but gradually became more abundant in PanINs and were highly abundant in invasive PDA (Fig. 3D). In KPC mice, Sema3D was primarily present in the cytoplasm and membrane of pancreatic tumor cells and was also present on the extracellular surface, possibly in a secreted form, whereas in KPCA$^{-/-}$ mice (which lacked *ANXA2* expression), Sema3D was modestly decreased in abundance, and its presence was localized primarily to the perinuclear

or nuclear regions of PDA tumor cells (Fig. 3E). In contrast, the localization of PlxnD1 and the localization of Sema3A, another member of the class 3 semaphorin family, were unaffected by *ANXA2* expression (Fig. 3F and fig. S4).

AnxA2 regulates the secretion of Sema3D from PDA cells

Class 3 semaphorins, including Sema3D, are secreted proteins (20). Our results thus far showed that tumor cells from KPCA$^{-/-}$ mice have decreased abundance of Sema3D compared to KPC cells that express *ANXA2*, but the extracellular Sema3D, which is possibly a secreted form of Sema3D, was also substantially decreased in these cells. Thus, we hypothesized that AnxA2 regulates the secretion of Sema3D rather than the expression of *SEMA3D* in PDA cells. To test this hypothesis, we first used enzyme-linked immunosorbent assay (ELISA) to measure the amount of secreted Sema3D in the cell culture supernatant, and found that the 24-hour secretion of Sema3D from KPCA$^{-/-}$ cells was significantly lower than that from KPC cells (Fig. 4A). This about 70-fold decrease in Sema3D secretion cannot be explained by the decrease in protein or RNA expression of Sema3D in KPCA$^{-/-}$ compared with KPC cells, because RNA expression was reduced by less than 10-fold (Fig. 3C). Rather, this result suggests that, in the absence of *ANXA2*, not only were the RNA and protein abundances of Sema3D decreased but also— and perhaps more importantly—the secretion of Sema3D was diminished. To confirm that AnxA2 mediated Sema3D secretion, we tested whether blockade of AnxA2 with function-blocking antibodies against AnxA2 (4) could suppress Sema3D secretion. We found that the addition of AnxA2 antibodies to KPC cells suppressed Sema3D secretion from these cells in a dose-dependent manner, whereas Sema3D secretion from KPCA$^{-/-}$ cells was unaffected (Fig. 4A). Similarly, small interfering RNA (siRNA) knockdown of *ANXA2* in KPC cells resulted in decreased Sema3D secretion (fig. S5). Therefore, these data support a role for AnxA2 in regulating the secretion of Sema3D from PDA cells.

To further understand the mechanism by which AnxA2 regulates the secretion of Sema3D, we examined whether an exocytosis inhibitor could inhibit the secretion of Sema3D because AnxA2 is known to play a role in exocytosis (21). We found that Sema3D secretion was inhibited in the presence of an exocytosis inhibitor (fig. S6A). The phosphorylation of Tyr^{23} in AnxA2 is important for the endocytic and exocytic functions of AnxA2 (22). We found that a Y23A mutant of *ANXA2*, which we previously reported to suppress PDA invasion and metastasis (4), largely inhibited the secretion of Sema3D from PDA cells (fig. S6B). Nonetheless, whether Sema3D secretion is mediated by the role of AnxA2 in exocytosis remains to be explored.

AnxA2 interacts with Sema3D and controls the complex formation between Sema3D and PlxnD1

To understand how AnxA2 mediates the secretion of Sema3D, we examined the protein-protein interaction between Sema3D and AnxA2 in PDA cells. Sema3D coimmunoprecipitated with AnxA2 in PDA cells (Fig. 4B), indicating that AnxA2 binds to Sema3D. Because AnxA2 is localized to the extracellular cell surface and is involved in exocytosis (21, 23, 24), AnxA2 may carry Sema3D to the cell surface for secretion.

The secreted form of Sema3D binds neuropilin 1 (NP-1) on the surface of mammalian cells (25), and the plexin family of proteins can act as co-receptors for semaphorins along with NP-1 by providing an intracellular domain to mediate intracellular signaling (26). However, the exact co-receptor for Sema3D is unknown. Therefore, we hypothesized that Sema3D, secreted from PDA cells, binds to the PlxnD1 co-receptor on the surface of PDA cells in an autocrine fashion. Supporting our hypothesis, coimmunoprecipitation assays indeed showed that PlxnD1 formed a complex with Sema3D in KPC PDA cells that express *ANXA2* (Fig. 4C). However, even though greater quantities of cell lysate from KPCA$^{-/-}$ cells were used for the coimmunoprecipitation assay to study equivalent amounts of both Sema3D and PlxnD1 proteins as was isolated from KPC PDA cells, PlxnD1 was unable to be coimmunoprecipitated from the KPCA$^{-/-}$ PDA cells, using antibodies against Sema3D. This result suggests that AnxA2 is required for Sema3D and PlxnD1 to form a complex, likely through controlling the secretion of Sema3D from PDA cells to facilitate the subsequent interaction between Sema3D and PlxnD1 on the surface of the tumor cell. Thus, in KPCA$^{-/-}$ cells lacking *ANXA2* expression, where Sema3D secretion is diminished, no Sema3D would bind to PlxnD1 on the surface of the cell.

Exogenous Sema3D can bind to PlxnD1 on the surface of the cell

To further demonstrate that Sema3D can bind to the cell surface of PDA cells via PlxnD1, we performed an alkaline phosphatase (AP) binding assay, which was previously used to study the binding between semaphorins and plexins on mammalians cells (25). *SEMA3E-AP* was used as a positive control for binding to PlxnD1 in the absence of NP-1, and NP-1 was used as a positive control for *SEMA3D-AP* binding, as described previously (fig. S7A) (25). *SEMA3D-AP* weakly and infrequently bound to the surface of COS7 cells transfected with a *PLXND1-VSV* plasmid but not to untransfected COS7 cells (Fig. 4D and fig. S7B). Nevertheless, stronger binding of Sema3D was observed on cells cotransfected with *PLXND1* and *NP-1*. We further confirmed the binding of Sema3D to NP-1 by coimmunoprecipitation in PDA cells (fig. S8). Because COS7 cells express *ANXA2* (27), KPC and KPCA$^{-/-}$ cells were also used in the AP binding assay to determine if AnxA2 is required for secreted Sema3D to bind to PlxnD1. Sema3D-AP bound PlxnD1 in both KPC and KPCA$^{-/-}$ cells (Fig. 4E). Together, these results indicate that AnxA2 promotes the secretion of Sema3D and that Sema3D, once secreted, binds PlxnD1 independently of AnxA2.

Knockdown of SEMA3D decreases the invasion and metastatic capacity of PDA cells and prolongs the survival of PDA-bearing mice

AnxA2 was previously shown to be required for PDA invasion and migration (4). Our new findings show that it also controls the secretion of Sema3D and, subsequently, the interaction between Sema3D and PlxnD1. Because both Sema3D and PlxnD1 are involved in cell motility (26), we examined whether Sema3D is also involved in PDA invasion and metastasis formation. To first test this in vitro, *SEMA3D* expression was knocked down with shRNA in the carcinogen-induced Panc02 PDA cells (Fig. 5A). The KPC cells were not used because of their leakage through the 8-μm filter in the Boyden invasion assay chamber. The invasion capacity of Panc02 cells was significantly decreased after SEMA3D knockdown in this in vitro invasion assay (Fig. 5B). The low invasive activity of PDA cells

with the *SEMA3D*-targeting shRNA was not due to a decrease in proliferation (fig. S9, A and B). In addition, nuclear localization of Snail-1, an EMT marker and a downstream effector of PlxnD1 (15), was decreased in SEMA3D knockdown cells in response to transforming growth factor–β [TGF-β, an inducer of EMT (4)] (fig. S10), further suggesting that the role of Sema3D in PDA invasion and EMT-associated migration is likely mediated by PlxnD1.

Next, we returned to the hemi-spleen liver metastasis model to determine whether knockdown of *SEMA3D* expression in KPC cells results in inhibition of the metastatic potential of KPC cells in vivo. KPC cells infected with lentivirus carrying the *SEMA3D*-targeting shRNA or those infected with control lentivirus were injected into the hemi-spleens of C57Bl/6 mice. Two weeks after tumor implant, extensive metastases were visualized in the livers of 11 of 12 mice receiving KPC cells infected with lentivirus carrying the control shRNA, whereas only small metastases were observed in 5 of 13 mice receiving KPC cells infected with the *SEMA3D*-targeting shRNA (Fig. 5C). Moreover, an independent experiment indicated that mice receiving KPC cells with the *SEMA3D*-targeting shRNA survived significantly longer than mice receiving KPC cells with the control shRNA (Fig. 5D). These results suggest that Sema3D is required for the homing and colonization steps of PDA metastasis.

To confirm a role of Sema3D in metastasis formation, we compared the growth rates of KPC cells with *SEMA3D* shRNA and KPC cells with control shRNA when KPC tumors were orthotopically implanted in the pancreas of syngeneic mice. Ultrasonic measurement of orthotopically implanted pancreatic tumors on days 6 and 20 after tumor implantation showed no significant difference in tumor development or growth rate between the tumors formed by KPC cells with *SEMA3D* shRNA and those formed by KPC cells with control shRNA (Fig. 5E and fig. S11, A and B). Furthermore, the tumor weights upon necropsy were not significantly different between the control shRNA and *SEMA3D* shRNA groups (fig. S12). In the control group of 10 mice, nine metastases were identified in the lung, liver, or peritoneum. However, in nine mice bearing tumors with *SEMA3D*-targeting shRNA, only two metastases were identified (Table 2). Therefore, Sema3D does appear to have a role in controlling PDA invasion and metastasis formation. Similar approaches also demonstrated a role of PlxnD1 in PDA invasion and metastasis formation (fig. S13, A to D).

Sema3D abundance is associated with metastasis formation in human PDA

To further establish the role of Sema3D in PDA metastasis formation, we performed Sema3D immunohistochemistry on human PDA tissue specimens. About 50% of surgically resected human PDAs had abundant Sema3D (in >50% of the tumor cells), whereas the remaining 50% of PDAs expressed low amounts of Sema3D (<5% of tumor cells) (Fig. 5F). Resected PDAs presenting with abundant Sema3D were observed in 15 of 20 patients (75%) with a disease-free survival (DFS) of <1 year, compared to only 4 of 15 patients (26.7%) with a DFS of >2 years (Fig. 5F), suggesting that Sema3D abundance in PDA is significantly associated with early recurrence after surgical resection. In all PDAs examined, Sema3D abundance positively correlated with PlxnD1 abundance, suggesting that Sema3D and PlxnD1 may be co-regulated (Fig. 5F). Using a unique human PDA tissue bank that

contains PDA specimens obtained from a rapid autopsy program, we found that 3 of 13 patients (23.1%) that died with local or oligometastatic disease had primary PDA tumors with abundant Sema3D, 14 of 22 patients (63.6%) with widely metastatic disease demonstrated abundant Sema3D in their primary PDA, and 17 of 22 patients (77.3%) with widely metastatic disease demonstrated abundant Sema3D in their metastatic tumors (Table 3). These results suggest that Sema3D is preferentially enriched in metastatic tumors of PDA and in primary PDAs from patients that have a poor prognosis or patients who died with widely metastatic disease.

Overexpression of SEMA3D partially reverses the defect in invasion and metastasis formation in ANXA2-deficient PDA cells

If Sema3D mediates the role of Anxa2 in PDA invasion and metastasis formation, we would anticipate that AnxA2-independent secretion of Sema3D may restore or partially restore the defect of *ANXA2*-deficient PDA cells in invasion and metastatic potential. To test this hypothesis, we knocked down *ANXA2* from Panc02 cells with *ANXA2*-targeting siRNA as described previously (4) and concurrently transfected the cells with a plasmid constitutively overexpressing SEMA3D through a cytomegalovirus promoter. We found that PDA cells transfected with this plasmid were able to secrete Sema3D at a reduced amount in the absence of *ANXA2* (fig. S14), although the exact mechanism for the secretion of this exogenously overexpressed SEMA3D remains to be explored. Panc02 cells transfected with scramble siRNA and/or an empty plasmid were used as a control. *ANXA2*-targeting siRNA significantly suppressed the invasion of Panc02 cells (Fig. 6A). However, overexpression of SEMA3D showed a trend but did not significantly restore the *ANXA2* siRNA–suppressed invasion capacity of Panc02 cells. Similarly, the addition of exogenous Sema3D-AP to the culture medium was also able to partially restore the *ANXA2* siRNA–suppressed invasion capacity of Panc02 cells (fig. S15); however, when PLXND1 was also knocked down by siRNA, Sema3D-AP was no longer able to restore this suppressed invasion capacity. This result further suggests that PlxnD1 mediates the role of Sema3D in PDA invasion.

Next, $KPCA^{-/-}$ cells were infected with GFP-encoding lentivirus carrying the mouse Sema3D, and their capacity to form liver metastases was tested in the hemi-spleen model. None of the mice receiving $KPCA^{-/-}$ cells infected with the same lentivirus expressing GFP alone formed liver metastases (Fig. 2). SEMA3D overexpression did not alter tumor cell proliferation rate (fig. S9C) or primary tumor growth (fig. S9D). However, 11 of 12 mice receiving $KPCA^{-/-}$ cells infected with lentivirus carrying both *SEMA3D* and *GFP* cDNAs developed liver metastases, assessed mid-assay by ultrasound (fig. S16) and assessed terminally at necropsy (Fig. 6B), suggesting that reintroduction of SEMA3D can largely restore the loss of metastatic potential in $KPCA^{-/-}$ cells. Together, these results suggest that Sema3D and PlxnD1 represent an AnxA2-downstream pathway that mediates the role of AnxA2 in PDA invasion and metastasis formation.

DISCUSSION

PDA is rarely controlled or cured by current therapeutic interventions because of a minimal understanding of the biologic processes that control its development, invasion, and

metastasis formation. Our study elucidated one mechanism of PDA metastasis formation that is mediated by AnxA2-dependent Sema3D secretion and subsequent autocrine activation of PlxnD1

Our previous study demonstrated that AnxA2 is involved in PDA metastasis formation in two murine tumor transplant models (4). Here, we used transgenic mice, which are genetically programmed to spontaneously develop PDA tumors in the same manner as human PDA, crossed with mice that have the *ANXA2* gene knocked out to enhance the evidence supporting a role for AnxA2 in PDA metastasis formation. Although knockout of *ANXA2* prevented metastases to liver and lungs, it did not alter the development of premalignant lesions and primary PDAs in this model, suggesting that the role of AnxA2 in metastasis may be mediated through a metastasis-specific pathway. Metastasis-specific pathways have been reported in breast cancer (28, 29) but have not yet been defined by the genetic engineered mouse model of PDA. We have not yet ruled out that our observations in *ANXA2*-null PDA tumors could be due to secondary biological changes; however, these results are consistent with the previously reported studies in which RNA interference of *ANXA2* produced a similar effect (4).

Sema3D and PlxnD1 were prioritized for further studies because these genes were found to be frequently altered at the genetic level in human PDAs (5). Our immunohistochemistry studies correlating the increase in abundance of Sema3D and PlxnD1 in human PDA metastases with poorer survival provide evidence suggesting that they likely are important for human PDA metastasis development. However, they are not the only downstream mediators. Overexpression of *SEMA3D* did not completely reverse the defects in PDA invasion and metastasis formation under *ANXA2* knockout or knockdown conditions, although it is also possible that over-expression of *SEMA3D* could not fully restore the abundance and kinetics of Sema3D secretion. Thus, it is important to explore other downstream pathways of AnxA2 in the future.

Our study shows that AnxA2 regulates the autocrine function of Sema3D by controlling its secretion, which makes Sema3D available in the extracellular space, where it binds PlxnD1 on the surface of PDA tumor cells (Fig. 6C). However, overexpression of *SEMA3D* was able to largely restore the function of Sema3D in the absence of AnxA2. Thus, future studies are required to delineate the mechanism and extent to which AnxA2 controls Sema3D secretion. Possibilities include genetic regulation of the gene and altered transport of the molecule within the tumor cell. Class 3 semaphorins colocalize with secretory vesicle proteins, such as Synaptobrevin (30), and AnxA2 has been implicated in vesicle trafficking and exocytosis (31). Thus, given these roles and our observation that Sema3D secretion is decreased after inhibition of exocytosis, it is possible that AnxA2 regulates the packaging of Sema3D into vesicles.

Future studies are also needed to clarify how the interaction of Sema3D with PlxnD1 functionally promotes tumor metastases. It is possible that Sema3D's autocrine function regulates PDA cell motility, considering the known functions of semaphorins and plexins in axon repulsion (32) as well as our previous report showing that AnxA2 regulates cell motility and EMT in both human and mouse PDA cells (4). Additionally, it is possible that

Sema3D may also act through a paracrine pathway because PlxnD1, its putative co-receptor, is also found on lymphovascular vessels and nerves (25, 33). A paracrine mechanism should be further studied because lymphovascular invasion and perineural invasion are two poor prognostic factors (34, 35) and are also proposed to be routes for cancer cells to metastasize along blood vessels, lymphatic vessels, and nerves (34, 35). Additionally, it will be interesting to explore whether the downstream signaling pathways that mediate the role of PlxnD1 in axon repulsion also mediate the role of AnxA2-Sema3D–PlxnD1 signaling in PDA invasion and metastasis. Previously, it was shown that the Sema3E–PlxnD1 interaction activates a signaling cascade downstream to the phosphorylation of the epidermal growth factor receptor family member ErbB2, specifically through activation of mitogen-activated protein kinase (MAPK) and phospholipase C-γ, which subsequently drives invasion and metastasis (10). Thus, it will be important to explore whether the Sema3D-PlxnD1 interaction also activates this signaling cascade during the PDA metastatic process.

In summary, this study has revealed a mechanistic role of axon guidance genes in PDA metastasis, and further studies are warranted to uncover the exact processes by which Sema3D and PlxnD1 induce invasion of PDA cells from the primary tumor site into the surrounding blood vessels, nerves, and lymphatic vessels. Nonetheless, this study provides a strong rationale for the development of new therapies targeting AnxA2 and Sema3D as an adjuvant treatment for PDA after local resection.

MATERIALS AND METHODS

Human PDA specimens

According to a Johns Hopkins Medical Institution (JHMI) Institutional Review Board (IRB)–approved protocol, archived PDA specimens were obtained from consecutive patients who underwent pancreaticoduodenectomy between 1998 and 2004 at Johns Hopkins Hospital (JHH) and received adjuvant chemoradiation therapy as previously described (36). Only patients who were primarily followed at JHH, with a DFS of >2 or <1 years, and whose archived paraffin-embedded tissue blocks were in good condition were included. In addition, a tissue microarray made from PDA specimens that were obtained from a JHMI IRB–approved rapid autopsy protocol was also included as previously described (37, 38).

Mouse models of PDA

All animal experiments conformed to the guidelines of the Animal Care and Use Committee of the Johns Hopkins University, and animals were maintained in accordance with the guidelines of the American Association of Laboratory Animal Care. All mice were monitored twice a day.

A genetically engineered mouse model of PDA, designated KPC mice, was previously established through a knock-in of pancreatic-specific, conditional alleles of the $KRAS^{G12D}$ and $TP53^{R172H}$ mutations on a mixed 129/SvJae/C57Bl/6 background. These mice, when crossed with $PDX\text{-}1\text{-}CRE^{+/+}$ mice, develop PanIN lesions that progress stepwise, similar to human disease, into PDA (16). The KPC mice were successfully backcrossed onto a C57Bl/6 background for nine generations. In addition to the KPC mice, *ANXA2*

homozygous knockout mice (*ANXA2*$^{-/-}$) on a C57Bl/6 background were also obtained (17) and crossed with the KPC mice to generate *KRAS*^{G12D} *TP53*^{R172H} *PDX-1-CRE*$^{+/+}$ *ANXA2*$^{-/-}$ (KPCA$^{-/-}$) mice.

The mouse hemi-spleen liver metastasis model has been previously described (19, 39). In short, the spleens of anesthetized female C57Bl/6 mice of ages 8 to 10 weeks were divided into two halves, and the halves were clipped. In total, 2×10^6 PDA cells were injected into the splenic vessels (splenic artery and veins) through one hemi-spleen followed by a flush of phosphate-buffered saline (PBS) buffer. After the injection, the splenic vessels draining the injected hemi-spleen were clipped, and the hemi-spleen was removed. The abdominal wall was sutured, and the skin was adapted using wound clips. All mice were followed twice daily for survival.

The mouse pancreatic orthotopic model was described previously (4). In brief, 2×10^6 PDA cells were subcutaneously injected into the flanks of syngeneic female C57Bl/6 mice. After 1 to 2 weeks, the subcutaneous tumors were harvested and cut into ~1-mm^3 pieces. New syngeneic female C57Bl/6 mice, ages 8 to 10 weeks, were anesthetized. The abdomen was opened via a left subcostal incision. A small pocket was prepared inside the pancreas using microscissors, into which one piece of the subcutaneous tumor was implanted. The incision in the pancreas was closed with a suture. The abdominal wall was sutured, and the skin was adapted using wound clips. Tumor size and metastasis formation were monitored at the indicated time points using small-animal ultrasound (Vevo770, VisualSonics).

Inferior vena cava model of lung metastases

The inferior vena cava (IVC) of anesthetized female C57Bl/6 mice of ages 8 to 10 weeks was exposed by making a midline incision into the peritoneum and moving the small and large intestines to one side. In total, 5×10^5 KPC or KPCA$^{-/-}$ cells were injected into the IVC at a position above the superior mesenteric vein. A sterile cotton swab was used to apply pressure for 2 to 3 min immediately after the injection to allow the blood to clot. The abdominal wall was sutured, and the skin was adapted using wound clips. All mice were followed twice daily. The mice were sacrificed 19 days after the IVC injection, and the lungs were harvested for histological analysis of metastasis formation. This model produces lung metastases more consistently than tail vein injection.

At necropsy, metastases were examined. Both macrometastases and mi-crometastases were scored for all metastatic evaluations. However, only the microscopic evaluations are presented here. The pancreas as well as the primary sites of metastases, including the liver, lung, and bowel, were removed and carefully sectioned for histological examination (fig. S17). All macrometastases observed during necropsy were confirmed upon histological analysis. Additional micrometastases were found in some mice upon histological examination of the tissue sections. Each experiment was repeated at least twice.

Development of KPC and KPCA$^{-/-}$ primary epithelial tumor cell lines

Pancreatic tumors were harvested from KPC or KPCA$^{-/-}$ mice into transport medium [RPMI 1640, penicillin (50 U/ml), streptomycin (50 μg/ml), gentamicin sulfate (10 μg/ml),

and fungizone (2.5 μg/ml); Invitrogen] and placed on ice. The tumors were diced using a surgical blade, placed in prewarmed digest medium [RPMI 1640, 5% fetal bovine serum (FBS), collagenase (1500 U/ml), and hyaluronidase (1000 U/ml); Invitrogen] and incubated at 37°C for 1 hour. After the digest, the tumor was filtered through a cell strainer (100 μm). The cells were spun at 1500 rpm for 10 min. All of the cells were plated in a 25-cm flask in primary pancreatic tumor medium [RPMI 1640, 10% FBS, 2 mM L-glutamine, 1% nonessential amino acids, 1 mM sodium pyruvate, penicillin (50 U/ml), and streptomycin (50 μg/ml); Invitrogen]. Two days later, the nonadherent cells were removed, and fresh primary pancreatic tumor medium was added to the flask. When the cells reached confluence, trypsin was added to the flask for 1 min to remove the fibroblasts. The fibroblasts were transferred to a new flask, and fresh medium was added to the original flask. This procedure was repeated until pure epithelial and fibroblast cell lines were obtained.

Cells

KPC and KPCA$^{-/-}$ cell lines were developed as described previously. Panc02 cells are a methylcholanthrene-induced pancreatic tumor cell line derived from C57Bl/6 mice (40). All mouse pancreatic tumor cells were maintained in RPMI 1640 medium containing 10% FBS, 1 mM sodium pyruvate, 2 mM L-glutamine, 1% nonessential amino acids (100×), penicillin (50 U/ml), and streptomycin (50 μg/ml) (Invitrogen) in a humidified incubator at 37°C, 5% CO_2. COS7 cells were maintained in Dulbecco's modified Eagle's medium containing 10% FBS in a humidified incubator at 37°C, 5% CO_2.

Cell proliferation

Cell proliferation was verified using cell counting kit-8 (CCK8). In brief, 2.5×10^5 tumor cells were plated in a six-well plate in complete medium. For the 0-hour time point, the medium was removed and replaced with 1 ml of fresh medium along with 100 μl of CCK8 reagent (Sigma) once the cells adhered to the plate. The plate was returned to the incubator for 2 hours and read at 450 nm on a SpectraMax M3 plate reader, using Softmax Pro v. 6.3 software (Molecular Devices). This procedure was repeated at 24 and 48 hours.

Quantitative RT-PCR

Pancreatic tumors were harvested from KPC and KPCA$^{-/-}$ mice, flash-frozen in liquid nitrogen or optimum cutting temperature compound (OCT), and stored at −80°C until RNA extraction was performed or slides were sectioned. RNA was extracted from flash-frozen pancreatic tissues using Trizol reagent. In brief, pancreatic tumors were diced in 1 ml of Trizol reagent and incubated at room temperature for 30 min. Chloroform was added (200 μl), and the samples were shaken vigorously for 15 s before incubation at room temperature for 2 min. Samples were spun at 12,000 rpm, and the aqueous phase was transferred to a fresh microcentrifuge tube. Isopropanol was added to the aqueous phase, and the samples were left at room temperature for 10 min. The samples were again centrifuged at 12,000 rpm, and the supernatant was removed. The RNA pellet was washed once in 75% ethanol, centrifuged at 9500 rpm, and left to air-dry for 30 min at room temperature. The RNA pellet was resuspended in 50 μl of distilled water, which was then added to a Qiagen Mini-Prep

RNA extraction column. Then, RNA purification was performed according to the manufacturer's instructions (Qiagen).

RNA was extracted from the frozen sections of pancreatic tumor embedded in OCT using Ambion's RNAqueous-Micro kit according to the manufacturer's protocol. qRT-PCR was performed on an Applied Biosystems RT-PCR machine (Life Technologies). All primers were obtained from Applied Biosystems (Life Technologies). Reactions were performed using Taq MasterMix (Life Technologies). All mRNA expression values were normalized to mouse *GAPDH* expression values.

Western blot analysis

Cells were lysed in 250 mM NaCl, 5 mM EDTA, 50 mM tris (pH 7.4), and 0.5% NP-40 containing protease inhibitors. After lysis, the lysate was spun at 15,000 rpm for 5 min. Samples boiled in SDS sample buffer containing reducing agents (Bio-Rad) were loaded and electrophoresed on a 4 to 12% bis-tris gel (Bio-Rad) for 2 hours at 120 V. The gels were transferred onto nitrocellulose membranes at 80 V for 1 hour at 4°C. The membranes were blocked in 5% bovine serum albumin (BSA) overnight at 4°C on a shaker. Primary antibodies were added in 2.5% BSA, and the membranes were incubated at room temperature for 2 hours. The membranes were washed and then incubated with rabbit or mouse secondary antibodies against horseradish peroxidase (1:5000; GE) for 1 hour at room temperature. The membranes were again washed and then developed using enhanced chemiluminescence reagent (GE).

Western blot analysis was performed using the following primary antibodies: a rabbit polyclonal antibody against Sema3D (1:1000; Abcam), a rabbit polyclonal antibody against AnxA2 (1:000; Santa Cruz Biotechnology), a rabbit polyclonal antibody against PlxnD1 (1:1000; Novus), or a mouse polyclonal antibody against β-actin (1:500; Santa Cruz Biotechnology).

Restoration of ANXA2 expression in the KPCA$^{-/-}$ cell line

The full-length mouse *ANXA2* cDNA (wild type and Y23A) (National Center for Biotechnology Information, GenBank: BC005763.1) was amplified using the following primers: forward, GCGTCTAGAATGTCTACTGTCCAC-GAAATCCTG; reverse, CGCGGATCCTCAGTCATCCCCACCACA-CAGGT. The amplicon was purified using the QIAquick PCR Purification Kit (Qiagen) and verified by sequencing. The QIAquick Gel Extraction Kit (Qiagen) was used to purify the PCR product, and the product was then ligated into a *pHIV-EGFP* plasmid. The plasmid was grown in an overnight culture under ampicillin selection and was then purified using the PureLink HiPure Plasmid Maxiprep Kit (Invitrogen). To produce lentivirus expressing mouse *ANXA2*, 293T cells were seeded in multiple six-well plates to 80% confluence. The plasmid containing *ANXA2* was cotransfected with packaging plasmids into 293T cells as previously described (41), using Lipofectamine 2000 (Invitrogen) in Opti-MEM medium. Lentiviral supernatant was collected at 48 hours. For infection, KPC cells were seeded in a 75-cm flask to 80% confluence. For each 75-cm flask, 5 ml of lentiviral supernatant was added with polybrene (5 μg/ml), and the cells were incubated for 48 hours before being harvested. The cells were

then analyzed by fluorescence-activated cell sorting (FACS) for GFP-positive cells and maintained in culture medium containing puromycin (0.25 μg/ml), which is a nonselecting dose. AnxA2 abundance in the sorted cells was confirmed by Western blot.

Overexpression of SEMA3D, shRNA knockdown of SEMA3D, and shRNA knockdown of PLXND1 in KPC cells

Lentivirus expressing mouse *SEMA3D* cDNA (pReceiver-Lv203, GeneCopoeia), mouse *SEMA3D* shRNA (GeneCopoeia), or mouse *PLXND1* shRNA (Thermo Scientific) was produced as described earlier. For infection, KPC cells were seeded in a 75-cm flask to 80% confluence. For each 75-cm flask, 5 ml of lentiviral supernatant was added with polybrene (5 μg/ml) and incubated for 48 hours before the cells were harvested. The cells were then analyzed by FACS for GFP-positive cells. Sema3D and PlxnD1 abundance in the sorted cells was assessed by Western blot.

Plasmid transfection and RNA interference

For plasmid transfection and RNA interference, cells were seeded in 10-cm dishes to 80% confluence. For each dish, 20 pmol of each siRNA duplex was transfected with Lipofectamine 2000 in serum-containing medium according to the manufacturer's instructions (Invitrogen). For invasion analysis, the culture medium was replaced with serum-free medium 24 hours after transfection, and the cells were harvested and plated in the invasion chamber 24 hours later. The *ANXA2* (4), *PLXND1*, and scramble siGENOME siRNAs were purchased from GE.

Microarray analysis

RNA was extracted from the KPC and KPCA$^{-/-}$ cell lines using the Qiagen RNA Mini Kit according to the manufacturer's instructions. Microarray analysis was performed at the Johns Hopkins Deep Sequencing and DNA Microarray Core using the Affymetrix MoEx Mouse Exon 1.0 ST array (Affymetrix). Data were extracted, RMA (robust multi-array average)–normalized, and analyzed for gene-level expression on the Partek Genomics Suite 6.6 platform (Partek Inc.). Gene Ontology analysis was performed using Spotfire DecisionSite with Functional Genomics Gene Ontology Browser (Tibco Spotfire Inc.). The genes that were increased or decreased in abundance by more than 1.5-fold were included for the analysis, which compared them to the universe of all the microarray's genes. The canonical pathways containing these genes were ranked by *P* values according to Fisher's exact test. The lower the *P* value is, the less likely these results could have occurred by chance, and thus, the more significantly the given pathway is enriched with genes that are either increased or decreased in abundance. We prioritized in our studies the two functional categories (cell movement pathway and cell morphology and remodeling pathway) that are the most significantly enriched with genes increased and decreased in abundance, respectively, because we are interested in studying the role of AnxA2 in invasion and metastasis. We then chose the six genes that were the most significantly increased or decreased in abundance from each of the two functional categories for further validation by RT-PCR in independent KPC and KPCA$^{-/-}$ tumor tissue.

Immunofluorescence

OCT-embedded frozen pancreatic tumors from KPC and KPCA$^{-/-}$ mice were sectioned and fixed in 4% paraformaldehyde for 10 min. The tumor sections were incubated in PBS containing 0.1% Triton X-100 for 5 min and then washed with PBS. Then, the tumor sections were blocked with 10% normal goat or donkey serum in PBS for 1 hour. Next, the tumor sections were incubated with antibodies against Sema3D (Abnova), PlxnD1 (Novus), Sema3A (Abcam), Snail1 (Abcam), NG2 (Chemicon), or AnxA2 (Cell Signaling) at a dilution of 1:25, 1:50 (Snail1), 1:300 (NG2), or 1:100 (AnxA2) in 10% normal goat or donkey serum overnight at 4°C. After the overnight incubation, the tumor sections were washed and were further incubated with FITC-conjugated goat antibodies against rabbit immunoglobulin G (IgG), FITC-conjugated goat antibodies against mouse IgG (Southern Biotechnology), or AF594-conjugated donkey antibodies against rabbit IgG (Life Technologies) at a 1:200 dilution or according to the manufacturer's instructions (AF594) in 10% normal goat or donkey serum at room temperature for 1 hour. NG2 staining was performed according to a previously described protocol (42). The tumor sections were subsequently washed and mounted in medium containing DAPI (4′,6-diamidino-2-phenylindole) (Vector Labs) before being examined under a fluorescence microscope.

Sema3D ELISA

Sema3D ELISA was performed according to the manufacturer's protocol (Cusabio). In brief, KPC and KPCA$^{-/-}$ cells were plated at 2.5×10^5 cells per well in a six-well plate. The next day, the medium was replaced with fresh medium containing the indicated amount of mouse monoclonal antibody against AnxA2 (clone Z014, both human and murine AnxA2-reactive; Invitrogen), and the cells were returned to the incubator for 24 hours. After incubation, the supernatant was removed from each well and spun at 1500 rpm for 5 min to remove any floating cells. The supernatant from the KPC cells was diluted 1:66 in the sample buffer provided in the kit, whereas the supernatant from the KPCA$^{-/-}$ cells was diluted 1:3 in the sample buffer. These dilutions were chosen because the final concentrations of Sema3D in these samples approximated 300 pg/ml, which falls in the middle of the standard curve.

Coimmunoprecipitation

Coimmunoprecipitation of AnxA2 and Sema3D was performed as follows. The Pierce Crosslink IP Kit (Thermo Scientific) was used to cross-link AnxA2 antibodies (BD Biosciences) to beads before performing coimmunoprecipitation according to the manufacturer's instructions with modifications. In brief, Protein A/G Plus agarose beads were loaded onto a column along with 5 μg of AnxA2 antibodies. Then, the column was incubated on a rotator for 60 min at room temperature. Next, after washing the beads three times with coupling buffer followed by centrifugation, 2.5 mM disuccinimidyl suberate was added to the column, and the cross-linking reaction was allowed to proceed for 1 hour on a rotator at room temperature. Then, the column was washed three times, and antibody cross-linking was confirmed by SDS–polyacrylamide gel electrophoresis (SDS-PAGE). Next, cell lysates were added to the cross-linked antibodies, and coimmunoprecipitation was performed at 4°C for 2 hours on a rotator. After the incubation, the column was washed, and

the beads were boiled in SDS buffer containing reducing agents. Finally, coimmunoprecipitates were analyzed by SDS-PAGE followed by Western blot.

Coimmunoprecipitation of Sema3D and PlxnD1 was performed as follows. First, rabbit polyclonal antibodies against Sema3D (Abcam) or rabbit polyclonal antibodies against IgG (Abcam) (1 μg) were added to the cell lysates and incubated for 2 hours on an end-over-end rotator at 4°C. Then, 100 μl of the Protein G Sepharose 4 Fast Flow bead slurry (GE) was added to the cell lysates in lysis buffer containing 150 mM NaCl, 50 mM tris (pH 7.4), and 1% NP-40. The lysate was incubated with the beads at 4°C overnight on an end-over-end rotator. Then, the beads were pelleted by pulse spin and washed five times (5 min each) in ice-cold lysis buffer [200 mM NaCl, 50 mM tris (pH 7.4), and 1% NP-40] on an end-over-end rotator. Finally, the beads were boiled in SDS sampling buffer containing reducing agents, and the coimmunoprecipitates were analyzed by SDS-PAGE followed by Western blot.

Coimmunoprecipitation of Sema3D and NP-1 was performed as follows. First, rabbit polyclonal antibodies against Sema3D (Abcam) or rabbit polyclonal antibodies against IgG (Abcam) (1 μg) were added to the cell lysates and incubated for 2 hours on an end-over-end rotator at 4° C. Then, 100 μl of the Protein G Sepharose 4 Fast Flow bead slurry (GE) was added to the cell lysates in lysis buffer containing 150 mM NaCl, 50 mM tris (pH 7.4), and 1% NP-40. The lysate was incubated with the beads at 4°C overnight on an end-over-end rotator. Then, the beads were pelleted by pulse spin and washed five times (5 min each) in ice-cold lysis buffer [200 mM NaCl, 50 mM tris (pH 7.4), and 1% NP-40] on an end-over-end rotator. Finally, the beads were boiled in SDS sampling buffer containing reducing agents, and the coimmunoprecipitates were analyzed by SDS-PAGE followed by Western blot.

Invasion assay

Invasion assays were performed using the Trevigen 96-well invasion assay kit according to the manufacturer's instructions with modifications (Trevigen). In brief, the Transwells were coated overnight with 1× basal membrane extract, and the cells were serum-starved 24 hours before the assay. Then, the cells were plated at 5×10^5 cells per well in triplicate in the top well of the Transwell plate. Invasion was measured 24 hours later using CCK8 (Sigma). Briefly, the cells in the top well were removed, and the wells were washed three times with the washing buffer provided in the kit. The top well of the Transwell plate was placed in a fresh 96-well plate containing 170 μl of complete cell medium and 17 μl of CCK8 reagent. The plate was returned to the incubator and incubated at 37°C, 5% CO_2 for 2 to 4 hours in the dark. After the incubation, the top chamber of the Transwell plate was removed, and the plate was read at 450 and 650 nm. Serum-free medium was added to the bottom well of the controls. CCK8 units were adjusted by subtracting the background invasion of the serum-free control from the experimental groups.

Immunohistochemistry

Immunohistochemistry staining for Sema3D and PlxnD1 was performed using a standard protocol on an automated stainer from Leica Microsystems. After deparaffinization and

hydration of tissue, heat-induced antigen retrieval was performed with EDTA buffer (pH 9.0) for 20 min. Incubation with rabbit antibodies against Sema3D (Abcam) at a 1:100 dilution or rabbit antibodies against PlxnD1 (Novus) at a 1:50 dilution for 30 min was followed by incubation with secondary antibody from the bond polymer REFINE detection kit (Leica Microsystems). The reaction was developed using the substrate 3,3'-diaminobenzidine hydrochloride (DAB; Vector Labs). All slides were counterstained with hematoxylin.

Immunohistochemistry for Ki67 and CD31 was performed manually. After deparaffinization and hydration of tissue, heat-induced antigen retrieval for Ki67 staining was performed in citrate buffer (pH 6.0) using a pressure cooker at 125°C for 30 s and 95°C for 10 s. Heat-induced antigen retrieval for CD31 staining was performed in EDTA buffer (pH 9.0) using a steamer for 1 hour at 97°C. Incubation with rabbit antibodies against Ki67 (Abcam) at a 1:500 dilution or rabbit antibodies against CD31 (Abcam) at a 1:100 dilution for 1 hour was followed by incubation with biotinylated secondary goat antibodies against rabbit IgG (Vector) at a 1:200 dilution for 30 min. After incubation with ABC Vectastain reagent (Vector), the reaction was developed using the DAB substrate (Vector Labs). All slides were counterstained with hematoxylin.

AP binding assay

The AP binding assay was performed as previously described (25). To produce the AP fusion proteins, COS7 cells (1.5×10^6) were transfected with 12 μg of plasmid DNA (*CTRL-AP*, *SEMA3D-AP*, or *SEMA3E-AP*), using Lipofectamine 2000 (Invitrogen) according to the manufacturer's protocol. Twenty-four hours after transfection, the culture medium was replaced with serum-free medium. Forty-eight hours after transfection, the supernatant was harvested from the cells and filtered using a 0.22-μm syringe filter. The amount of AP-tagged ligand in the supernatant was measured using a colorimetric AP assay kit (Abcam). Next, the supernatant containing the AP fusion proteins was added to COS7 cells (2.5×10^5), which were transfected with 2 μg of *PLXND1* or *NP-1* per well for 48 hours in a six-well plate, for 75 min with gentle rocking at room temperature. After incubation, the cells were washed six times with HBH [1× Hanks' balanced salt solution, 0.05% BSA, 20 mM Hepes (pH 7.0), 6 mM calcium chloride, and 2 mM magnesium chloride]. Next, the cells were fixed in 60% acetone, 3% formaldehyde, and 20 mM Hepes (pH 7.0) for 1 min. Then, the cells were washed three times with HBH, and the HBH was replaced with HBS [20 mM Hepes (pH 7.0) and 150 mM NaCl]. Endogenous AP was inactivated by incubating in a humidified chamber at 65°C for 110 min. Finally, AP was visualized using AP stain [100 mM tris (pH 9.5), 100 mM NaCl, 5 mM $MgCl_2$, nitroblue tetrazolium (0.33 mg/ml), and 5-bromo,4-chloro,3-indolylphosphate (0.17 mg/ml)]. The stained cells were visualized under a microscope.

TUNEL assay

The TUNEL (terminal deoxynucleotidyl transferase-mediated deoxyuridine triphosphate nick end labeling) assay was performed according to the manufacturer's instructions (Roche).

Inhibition of exocytosis

KPC cells were plated to 80% confluence in 10-cm culture dishes. Before beginning the assay, the culture medium was replaced with fresh serum-containing pancreatic tumor cell medium. GolgiPlug (brefeldin A; BD Biosciences) was added to the fresh culture medium at a concentration of 1 μl/ml of culture medium. Five hours later, the cell supernatant was removed, spun at 1500 rpm for 5 min, and frozen at −80°C until analyzed using the Sema3D ELISA kit.

Statistical analysis

Statistical analysis was performed using GraphPad Prism version 6.0 software (GraphPad Software). Fisher's exact test was used to compare differences between treatment groups. Linear regression analysis was used to compare Sema3D secretion between KPC and KPCA$^{-/-}$ cell lines after AnxA2 antibody inhibition, as well as the proliferation rates of different cell lines. Mouse survival was analyzed by the Kaplan-Meier method and the log-rank test. A P value of <0.05 was considered statistically significant.

Supplementary Material

Refer to Web version on PubMed Central for supplementary material.

Acknowledgments

We thank D. Ginty for providing us with valuable reagents and his technical consultations. We thank H. Zhao at the flow cytometry core and C. Talbot at the microarray core for their technical support. We thank E. Sugar at the Johns Hopkins University School of Public Health for her statistical consultation and critiques of our manuscript. **Funding**: This work was supported in part by NIH grant R01 CA169702 (L.Z.); NIH grant K23 CA148964-01 (L.Z.); the Viragh Foundation and the Skip Viragh Pancreatic Cancer Center at Johns Hopkins (E.M.J. and L.Z.); the Lefkofsky Family Foundation (L.Z.); National Cancer Institute Specialized Programs of Research Excellence in Gastrointestinal Cancers grant P50 CA062924 (E.M.J. and L.Z.); Sidney Kimmel Comprehensive Cancer Center grant P30 CA006973 (E.M.J.); NIH grant HL42093 (K.A.H.); MOD FY15-226 (K.A.H.); and a Lustgarten Foundation grant (L.Z.).

E.M.J. receives research funding from Roche and Aduro Biotech.

REFERENCES AND NOTES

1. Siegel R, Ma J, Zou Z, Jemal A. Cancer statistics, 2014. CA Cancer J. Clin. 2014; 64:9–29. [PubMed: 24399786]
2. Li D, Xie K, Wolff R, Abbruzzese JL. Pancreatic cancer. Lancet. 2004; 363:1049–1057. [PubMed: 15051286]
3. Lutz E, Yeo CJ, Lillemoe KD, Biedrzycki B, Kobrin B, Herman J, Sugar E, Piantadosi S, Cameron JL, Solt S, Onners B, Tartakovsky I, Choi M, Sharma R, Illei PB, Hruban RH, Abrams RA, Le D, Jaffee E, Laheru D. A lethally irradiated allogeneic granulocyte-macrophage colony stimulating factor-secreting tumor vaccine for pancreatic adenocarcinoma. A phase II trial of safety, efficacy, and immune activation. Ann. Surg. 2011; 253:328–335. [PubMed: 21217520]
4. Zheng L, Foley K, Huang L, Leubner A, Mo G, Olino K, Edil BH, Mizuma M, Sharma R, Le DT, Anders RA, Illei PB, Van Eyk JE, Maitra A, Laheru D, Jaffee EM. Tyrosine 23 phosphorylation-dependent cell-surface localization of annexin A2 is required for invasion and metastases of pancreatic cancer. PLOS One. 2011; 6:e19390. [PubMed: 21572519]
5. Biankin AV, Waddell N, Kassahn KS, Gingras MC, Muthuswamy LB, Johns AL, Miller DK, Wilson PJ, Patch AM, Wu J, Chang DK, Cowley MJ, Gardiner BB, Song S, Harliwong I, Idrisoglu S, Nourse C, Nourbakhsh E, Manning S, Wani S, Gongora M, Pajic M, Scarlett CJ, Gill AJ, Pinho

AV, Rooman I, Anderson M, Holmes O, Leonard C, Taylor D, Wood S, Xu Q, Nones K, Fink JL, Christ A, Bruxner T, Cloonan N, Kolle G, Newell F, Pinese M, Mead RS, Humphris JL, Kaplan W, Jones MD, Colvin EK, Nagrial AM, Humphrey ES, Chou A, Chin VT, Chantrill LA, Mawson A, Samra JS, Kench JG, Lovell JA, Daly RJ, Merrett ND, Toon C, Epari K, Nguyen NQ, Barbour A, Zeps N, Australian Pancreatic Cancer Genome I, Kakkar N, Zhao F, Wu YQ, Wang M, Muzny DM, Fisher WE, Brunicardi FC, Hodges SE, Reid JG, Drummond J, Chang K, Han Y, Lewis LR, Dinh H, Buhay CJ, Beck T, Timms L, Sam M, Begley K, Brown A, Pai D, Panchal A, Buchner N, De Borja R, Denroche RE, Yung CK, Serra S, Onetto N, Mukhopadhyay D, Tsao MS, Shaw PA, Petersen GM, Gallinger S, Hruban RH, Maitra A, Iacobuzio-Donahue CA, Schulick RD, Wolfgang CL, Morgan RA, Lawlor RT, Capelli P, Corbo V, Scardoni M, Tortora G, Tempero MA, Mann KM, Jenkins NA, Perez-Mancera PA, Adams DJ, Largaespada DA, Wessels LF, Rust AG, Stein LD, Tuveson DA, Copeland NG, Musgrove EA, Scarpa A, Eshleman JR, Hudson TJ, Sutherland RL, Wheeler DA, Pearson JV, McPherson JD, Gibbs RA, Grimmond SM. Pancreatic cancer genomes reveal aberrations in axon guidance pathway genes. Nature. 2012; 491:399–405. [PubMed: 23103869]

6. Jones S, Zhang X, Parsons DW, Lin JC, Leary RJ, Angenendt P, Mankoo P, Carter H, Kamiyama H, Jimeno A, Hong SM, Fu B, Lin MT, Calhoun ES, Kamiyama M, Walter K, Nikolskaya T, Nikolsky Y, Hartigan J, Smith DR, Hidalgo M, Leach SD, Klein AP, Jaffee EM, Goggins M, Maitra A, Iacobuzio-Donahue C, Eshleman JR, Kern SE, Hruban RH, Karchin R, Papadopoulos N, Parmigiani G, Vogelstein B, Velculescu VE, Kinzler KW. Core signaling pathways in human pancreatic cancers revealed by global genomic analyses. Science. 2008; 321:1801–1806. [PubMed: 18772397]
7. Müller MW, Giese NA, Swiercz JM, Ceyhan GO, Esposito I, Hinz U, Büchler P, Giese T, Büchler MW, Offermanns S, Friess H. Association of axon guidance factor semaphorin 3A with poor outcome in pancreatic cancer. Int. J. Cancer. 2007; 121:2421–2433. [PubMed: 17631638]
8. Roodink I, Kats G, van Kempen L, Grunberg M, Maass C, Verrijp K, Raats J, Leenders W. Semaphorin 3E expression correlates inversely with plexin D1 during tumor progression. Am. J. Pathol. 2008; 173:1873–1881. [PubMed: 18974298]
9. Shalaby MA, Hampson L, Oliver A, Hampson I. Plexin D1: New potential biomarker for cervical cancer. J. Immunoassay Immunochem. 2012; 33:223–233. [PubMed: 22738647]
10. Casazza A, Finisguerra V, Capparuccia L, Camperi A, Swiercz JM, Rizzolio S, Rolny C, Christensen C, Bertotti A, Sarotto I, Risio M, Trusolino L, Weitz J, Schneider M, Mazzone M, Comoglio PM, Tamagnone L. Sema3E–Plexin D1 signaling drives human cancer cell invasiveness and metastatic spreading in mice. J. Clin. Invest. 2010; 120:2684–2698. [PubMed: 20664171]
11. Luchino J, Hocine M, Amoureux MC, Gibert B, Bemet A, Royet A, Treilleux I, Lécine P, Borg JP, Mehlen P, Chauvet S, Mann F. Semaphorin 3E suppresses tumor cell death triggered by the plexin D1 dependence receptor in metastatic breast cancers. Cancer Cell. 2013; 24:673–685. [PubMed: 24139859]
12. Mehlen P, Delloye-Bourgeois C, Chédotal A. Novel roles for Slits and netrins: Axon guidance cues as anticancer targets? Nat. Rev. Cancer. 2011; 11:188–197. [PubMed: 21326323]
13. Worzfeld T, Offermanns S. Semaphorins and plexins as therapeutic targets. Nat. Rev. Drug Discov. 2014; 13:603–621. [PubMed: 25082288]
14. Rehman M, Tamagnone L. Semaphorins in cancer: Biological mechanisms and therapeutic approaches. Semin. Cell Dev. Biol. 2013; 24:179–189. [PubMed: 23099250]
15. Tseng CH, Murray KD, Jou MF, Hsu SM, Cheng HJ, Huang PH. Sema3E/plexin-D1 mediated epithelial-to-mesenchymal transition in ovarian endometrioid cancer. PLOS One. 2011; 6:e19396. [PubMed: 21559368]
16. Hingorani SR, Wang L, Multani AS, Combs C, Deramaudt TB, Hruban RH, Rustgi AK, Chang S, Tuveson DA. *Trp53*^{R172H} and *Kras*^{G12D} cooperate to promote chromosomal instability and widely metastatic pancreatic ductal adenocarcinoma in mice. Cancer Cell. 2005; 7:469–483. [PubMed: 15894267]
17. Ling Q, Jacovina AT, Deora A, Febbraio M, Simantov R, Silverstein RL, Hempstead B, Mark WH, Hajjar KA. Annexin II regulates fibrin homeostasis and neoangiogenesis in vivo. J. Clin. Invest. 2004; 113:38–48. [PubMed: 14702107]
18. Huang B, Deora AB, He KL, Chen K, Sui G, Jacovina AT, Almeida D, Hong P, Burgman P, Hajjar KA. Hypoxia-inducible factor-1 drives annexin A2 system-mediated perivascular fibrin

clearance in oxygen-induced retinopathy in mice. Blood. 2011; 118:2918–2929. [PubMed: 21788340]

19. Soares KC, Foley K, Olino K, Leubner A, Mayo SC, Jain A, Jaffee E, Schulick RD, Yoshimura K, Edil B, Zheng L. A preclinical murine model of hepatic metastases. J. Vis. Exp. 2014; 91:51677. [PubMed: 25285458]
20. Tamagnone L, Comoglio PM. To move or not to move? Semaphorin signalling in cell migration. EMBO Rep. 2004; 5:356–361. [PubMed: 15060572]
21. Gerke V, Moss SE. Annexins: From structure to function. Physiol. Rev. 2002; 82:331–371. [PubMed: 11917092]
22. Biener Y, Feinstein R, Mayak M, Kaburagi Y, Kadowaki T, Zick Y. Annexin II is a novel player in insulin signal transduction. Possible association between annexin II phosphorylation and insulin receptor internalization. J. Biol. Chem. 1996; 271:29489–29496. [PubMed: 8910617]
23. Drust DS, Creutz CE. Aggregation of chromaffin granules by calpactin at micromolar levels of calcium. Nature. 1988; 331:88–91. [PubMed: 2963226]
24. Geisow MJ, Walker JH, Boustead C, Taylor W. Annexins—New family of Ca^{2+}-regulated-phospholipid binding protein. Biosci. Rep. 1987; 7:289–298. [PubMed: 2960386]
25. Gu C, Yoshida Y, Livet J, Reimert DV, Mann F, Merte J, Henderson CE, Jessell TM, Kolodkin AL, Ginty DD. Semaphorin 3E and plexin-D1 control vascular pattern independently of neuropilins. Science. 2005; 307:265–268. [PubMed: 15550623]
26. Tamagnone L, Comoglio PM. Signalling by semaphorin receptors: Cell guidance and beyond. Trends Cell Biol. 2000; 10:377–383. [PubMed: 10932095]
27. Oh YS, Gao P, Lee KW, Ceglia I, Seo JS, Zhang X, Ahn JH, Chait BT, Patel DJ, Kim Y, Greengard P. SMARCA3, a chromatin-remodeling factor, is required for p11-dependent antidepressant action. Cell. 2013; 152:831–843. [PubMed: 23415230]
28. Minn AJ, Gupta GP, Siegel PM, Bos PD, Shu W, Giri DD, Viale A, Olshen AB, Gerald WL, Massagué J. Genes that mediate breast cancer metastasis to lung. Nature. 2005; 436:518–524. [PubMed: 16049480]
29. Rodenhiser DI, Andrews JD, Vandenberg TA, Chambers AF. Gene signatures of breast cancer progression and metastasis. Breast Cancer Res. 2011; 13:201. [PubMed: 21345283]
30. Zylbersztejn K, Petkovic M, Burgo A, Deck M, Garel S, Marcos S, Bloch-Gallego E, Nothias F, Serini G, Bagnard D, Binz T, Galli T. The vesicular SNARE Synaptobrevin is required for Semaphorin 3A axonal repulsion. J. Cell Biol. 2012; 196:37–46. [PubMed: 22213797]
31. Merrifield CJ, Rescher U, Almers W, Proust J, Gerke V, Sechi AS, Moss SE. Annexin 2 has an essential role in actin-based macropinocytic rocketing. Curr. Biol. 2001; 11:1136–1141. [PubMed: 11509239]
32. Yazdani U, Terman JR. The semaphorins. Genome Biol. 2006; 7:211. [PubMed: 16584533]
33. Pecho-Vrieseling E, Sigrist M, Yoshida Y, Jessell TM, Arber S. Specificity of sensory-motor connections encoded by Sema3e-Plxnd1 recognition. Nature. 2009; 459:842–846. [PubMed: 19421194]
34. Bapat AA, Hostetter G, Von Hoff DD, Han H. Perineural invasion and associated pain in pancreatic cancer. Nat. Rev. Cancer. 2011; 11:695–707. [PubMed: 21941281]
35. Takahashi H, Ohigashi H, Ishikawa O, Gotoh K, Yamada T, Nagata S, Tomita Y, Eguchi H, Doki Y, Yano M. Perineural invasion and lymph node involvement as indicators of surgical outcome and pattern of recurrence in the setting of preoperative gemcitabine-based chemoradiation therapy for resectable pancreatic cancer. Ann. Surg. 2012; 255:95–102. [PubMed: 22123160]
36. Bever KM, Sugar EA, Bigelow E, Sharma R, Laheru D, Wolfgang CL, Jaffee EM, Anders RA, De Jesus-Acosta A, Zheng L. The prognostic value of stroma in pancreatic cancer in patients receiving adjuvant therapy. HPB. 2015; 17:292–298. [PubMed: 25250696]
37. Iacobuzio-Donahue CA, Fu B, Yachida S, Luo M, Abe H, Henderson CM, Vilardell F, Wang Z, Keller JW, Banerjee P, Herman JM, Cameron JL, Yeo CJ, Halushka MK, Eshleman JR, Raben M, Klein AP, Hruban RH, Hidalgo M, Laheru D. DPC4 gene status of the primary carcinoma correlates with patterns of failure in patients with pancreatic cancer. J. Clin. Oncol. 2009; 27:1806–1813. [PubMed: 19273710]

38. Pérez-Mancera PA, Rust AG, van der Weyden L, Kristiansen G, Li A, Sarver AL, Silverstein KA, Grützmann R, Aust D, Rümmele P, Knösel T, Herd C, Stemple DL, Kettleborough R, Brosnan JA, Li A, Morgan R, Knight S, Yu J, Stegeman S, Collier LS, ten Hoeve JJ, de Ridder J, Klein AP, Goggins M, Hruban RH, Chang DK, Biankin AV, Grimmond Australian Pancreatic Cancer Genome SM, Wessels LF, Wood SA, Iacobuzio-Donahue CA, Pilarsky C, Largaespada DA, Adams DJ, Tuveson DA. The deubiquitinase USP9X suppresses pancreatic ductal adenocarcinoma. Nature. 2012; 486:266–270. [PubMed: 22699621]

39. Jain A, Slansky JE, Matey LC, Allen HE, Pardoll DM, Schulick RD. Synergistic effect of a granulocyte-macrophage colony-stimulating factor-transduced tumor vaccine and systemic interleukin-2 in the treatment of murine colorectal cancer hepatic metastases. Ann. Surg. Oncol. 2003; 10:810–820. [PubMed: 12900373]

40. Corbett TH, Roberts BJ, Leopold WR, Peckham JC, Wilkoff LJ, Griswold DP Jr, Schabel FM Jr. Induction and chemotherapeutic response of two transplantable ductal adenocarcinomas of the pancreas in C57BL/6 mice. Cancer Res. 1984; 44:717–726. [PubMed: 6692374]

41. Zhou X, Cui Y, Huang X, Yu Z, Thomas AM, Ye Z, Pardoll DM, Jaffee EM, Cheng L. Lentivirus-mediated gene transfer and expression in established human tumor antigen-specific cytotoxic T cells and primary unstimulated T cells. Hum. Gene Ther. 2003; 14:1089–1105. [PubMed: 12885348]

42. Ruan J, Luo M, Wang C, Fan L, Yang SN, Cardenas M, Geng H, Leonard JP, Melnick A, Cerchietti L, Hajjar KA. Imatinib disrupts lymphoma angiogenesis by targeting vascular pericytes. Blood. 2013; 121:5192–5202. [PubMed: 23632889]

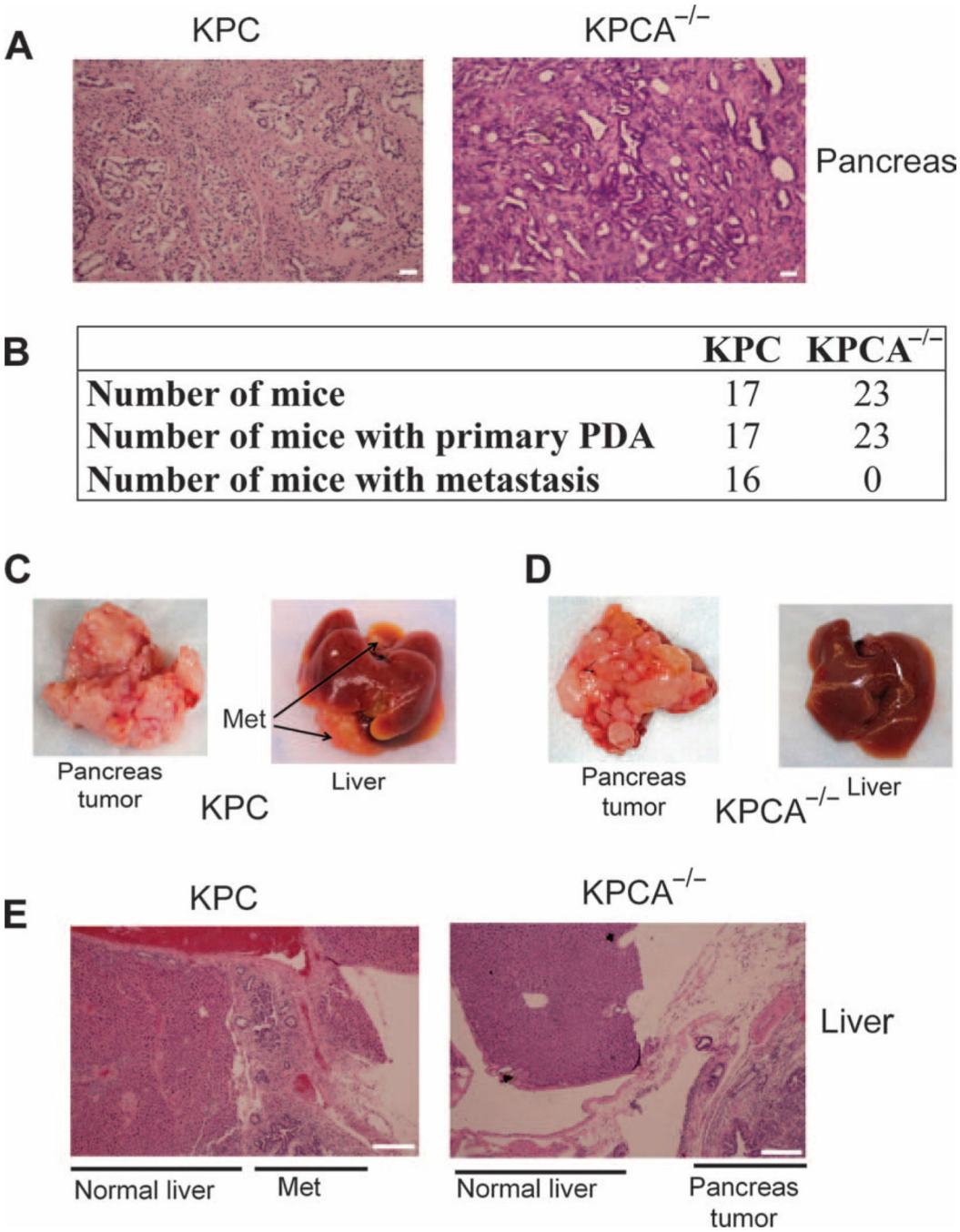

	KPC	KPCA$^{-/-}$
Number of mice	17	23
Number of mice with primary PDA	17	23
Number of mice with metastasis	16	0

Fig. 1. *ANXA2* is essential for PDA metastasis formation in a transgenic mouse model of PDA

(**A**) Hematoxylin and eosin (H&E) staining of PDA from representative KPC and KPCA$^{-/-}$ mice. (**B**) Tabulated summary of histologically confirmed primary PDA and metastases formed in *KRAS*^{G12D} *TP53*^{R172H} *PDX-1-CRE*$^{+/+}$ (KPC) and *KRAS*^{G12D} *TP53*^{R172H} *PDX-1-CRE*$^{+/+}$ *ANXA2*$^{-/-}$ (KPCA$^{-/-}$) mice. All mice in both cohorts developed primary PDA. Gross metastases to the liver were observed in 16 of 17 KPC mice with primary pancreatic tumors. However, none of the KPCA$^{-/-}$ mice (0 of 23) developed metastases to the liver ($P < 0.001$, Fisher's exact test). (**C**) Gross images of a primary pancreatic tumor and liver from

a representative 6-month-old KPC mouse. (**D**) Gross images of a primary pancreatic tumor and liver from a representative 6-month-old KPCA$^{-/-}$ mouse. (**E**) H&E staining of PDA from representative KPC and KPCA$^{-/-}$ mice showing invasive metastases in the liver of the KPC mouse but no invasion of the pancreatic tumor into the liver of the KPCA$^{-/-}$ mouse. Scale bars, 200 μm. Images in all panels are representative of at least 17 mice.

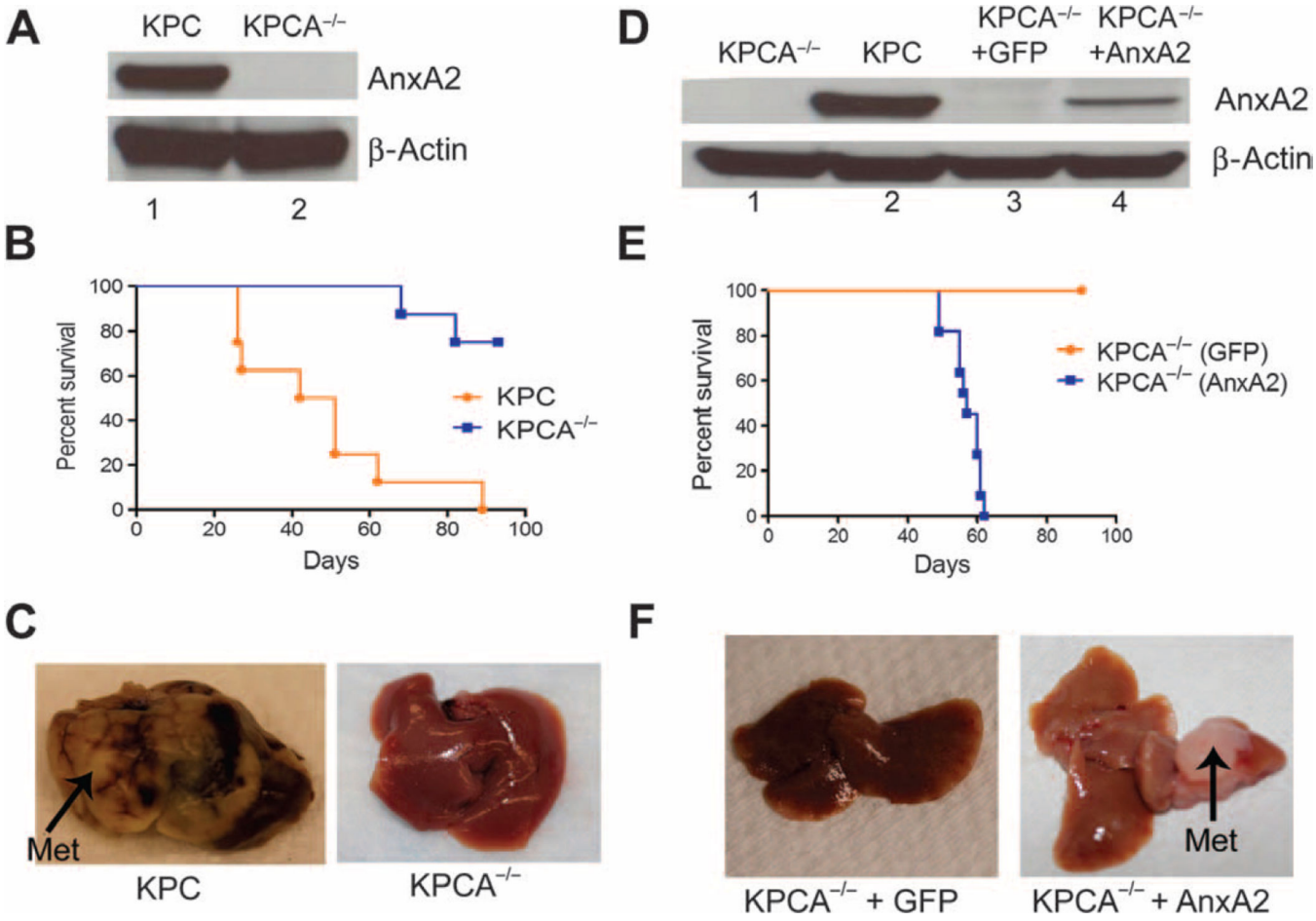

Fig. 2. Reintroduction of *ANXA2* is able to restore the metastatic potential of *ANXA2*$^{-/-}$ PDA cells

(**A**) Western blotting for AnxA2 in primary pancreatic tumor lines developed from KPC and KPCA$^{-/-}$ mice. Blots are representative of at least three experiments. (**B**) Kaplan-Meier analysis of mice that received a hemi-spleen injection of KPC or KPCA$^{-/-}$ cells (n = 10 mice per group) (P < 0.001, log-rank test). (**C**) Detection of gross metastatic lesions in the livers of mice that received splenic injection of KPC or KPCA$^{-/-}$ cells. Images are representative of 10 mice. (**D**) Western blot analysis demonstrating successful knock-in of *ANXA2* expression into KPCA$^{-/-}$ cells. β-Actin was used as a loading control. Blots are representative of at least three experiments. (**E**) Kaplan-Meier analysis of mice that received a hemi-spleen injection of KPCA$^{-/-}$ + *GFP* or KPCA$^{-/-}$ + *ANXA2* cells (n = 11 mice per group) (P < 0.001, log-rank test). (**F**) Formation of liver lesions by KPCA$^{-/-}$ + *ANXA2* or KPCA$^{-/-}$ + *GFP* cells. Scale bars, 20 μm. Images are representative of 11 mice.

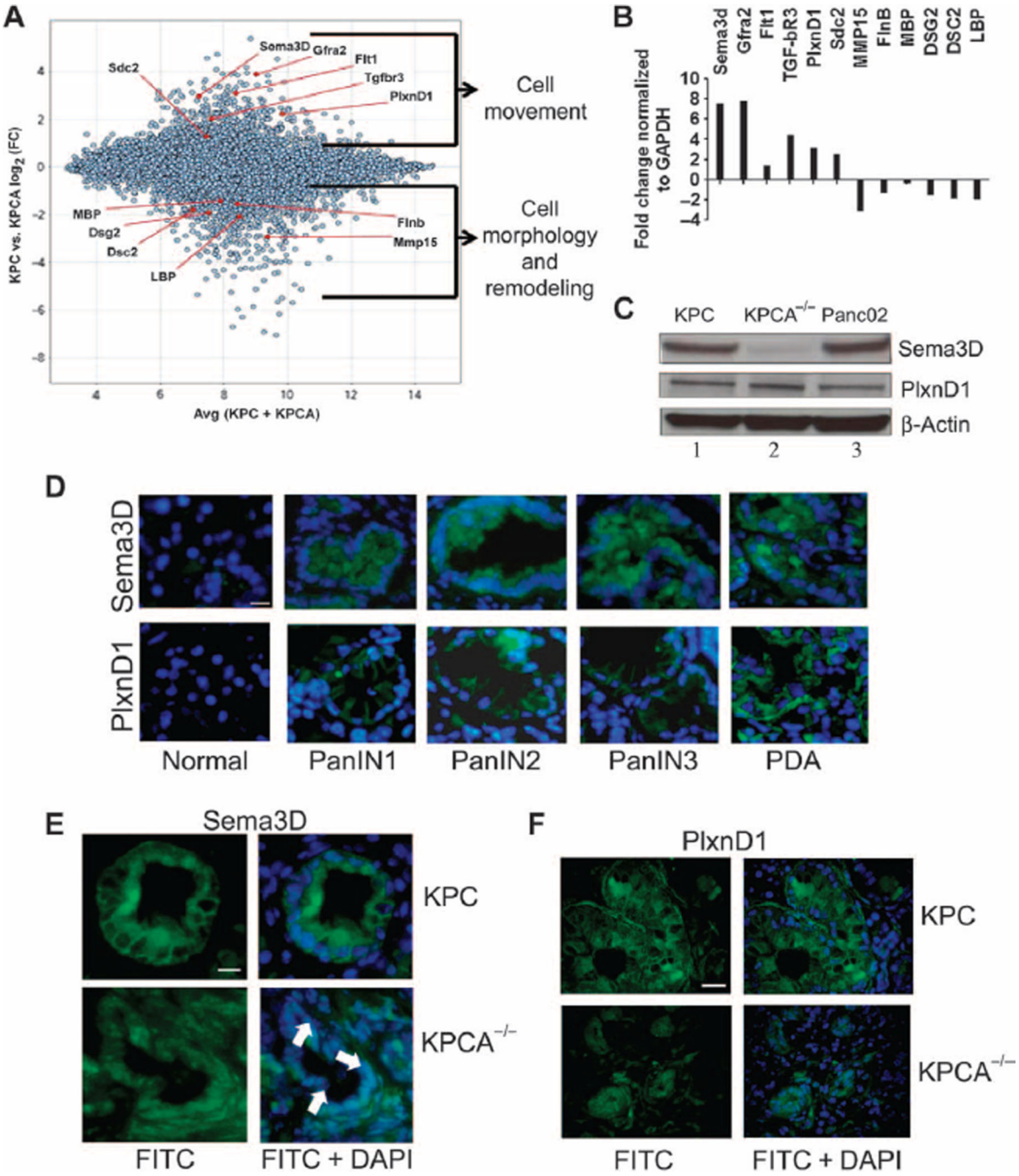

Fig. 3. The abundance of Sema3D is differentially regulated in pancreatic tumors from KPCA$^{-/-}$ and KPC mice

(**A**) A plot showing the six genes involved in cell movement (top) and cell morphology and remodeling (bottom) that had the highest fold change difference in gene expression between KPC and KPCA$^{-/-}$ cells ($P < 0.001$, hypergeometric and Fisher's exact tests). (**B**) qRT-PCR validation of the microarray data in independent tumor samples obtained from KPC and KPCA$^{-/-}$ mice. Data are mean fold change of KPC versus KPCA$^{-/-}$ normalized to glyceraldehyde-3-phosphate dehydrogenase (GAPDH) amounts from 12 independent tumors

per group. (**C**) Western blot analysis of Sema3D and PlxnD1 abundance in KPC, KPCA$^{-/-}$, and Panc02 pancreatic tumor cell lines. Blots are representative of at least two experiments. (**D**) Immunofluorescence analysis of Sema3D and PlxnD1 during pancreatic tumor progression. (**E**) Immunofluorescence staining of Sema3D [fluorescein isothiocyanate (FITC)] in PanINs from KPC and KPCA$^{-/-}$ mice. (**F**) Immunofluorescence staining of PlxnD1 (FITC) in PanINs from KPC and KPCA$^{-/-}$ mice. Scale bars, 20 μm. Images in (D) to (F) are representative of at least 10 mice.

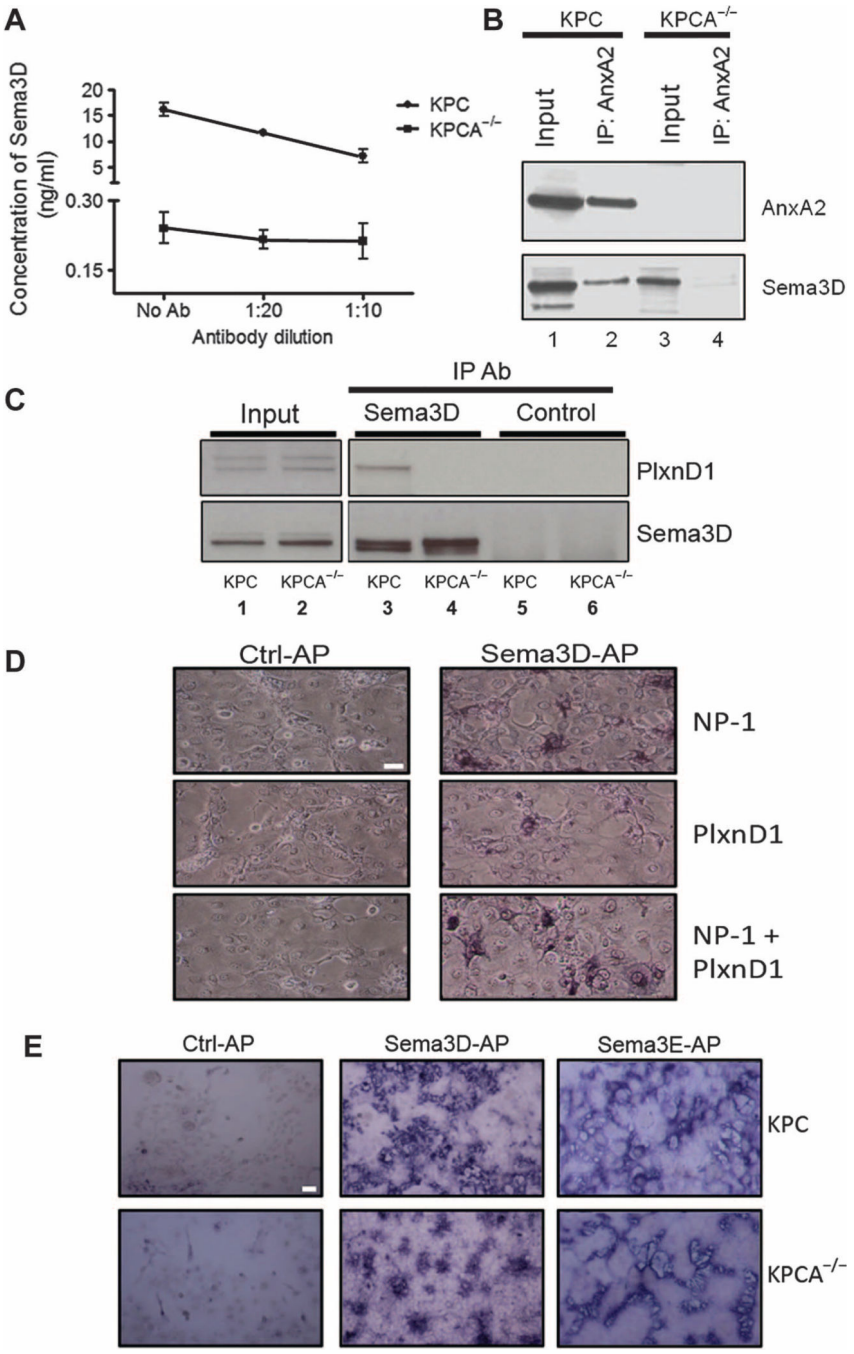

Fig. 4. AnxA2 controls the secretion of Sema3D from PDA cells, allowing it to interact with its receptor, PlxnD1, in an AnxA2-dependent manner

(**A**) Sema3D secretion in KPC and KPCA$^{-/-}$ cells was determined by ELISA ($P < 0.031$ for all, KPC versus KPCA; linear regression analysis), with and without the addition of antibodies against AnxA2. Data are means ± SEM from three independent biological replicates. (**B**) Coimmunoprecipitation and Western blot analysis of AnxA2 and Sema3D in KPC cells. KPCA$^{-/-}$ cells were used as a control. (**C**) Coimmunoprecipitation and Western blot analysis of PlxnD1 and Sema3D in KPC cells. Blots in (B) and (C) are representative of

at least two experiments. (**D**) Sema3D-AP binds to NP-1, PlxnD1, and PlxnD1 in the presence of NP-1. (**E**) Exogenous Sema3D-AP binds to PlxnD1 on the surface of both KPC and KPCA$^{-/-}$ cells. Sema3E-AP was used as a control. All images were acquired at ×20 magnification. Scale bars, 20 μm. Images in (D) and (E) are representative of at least three experiments.

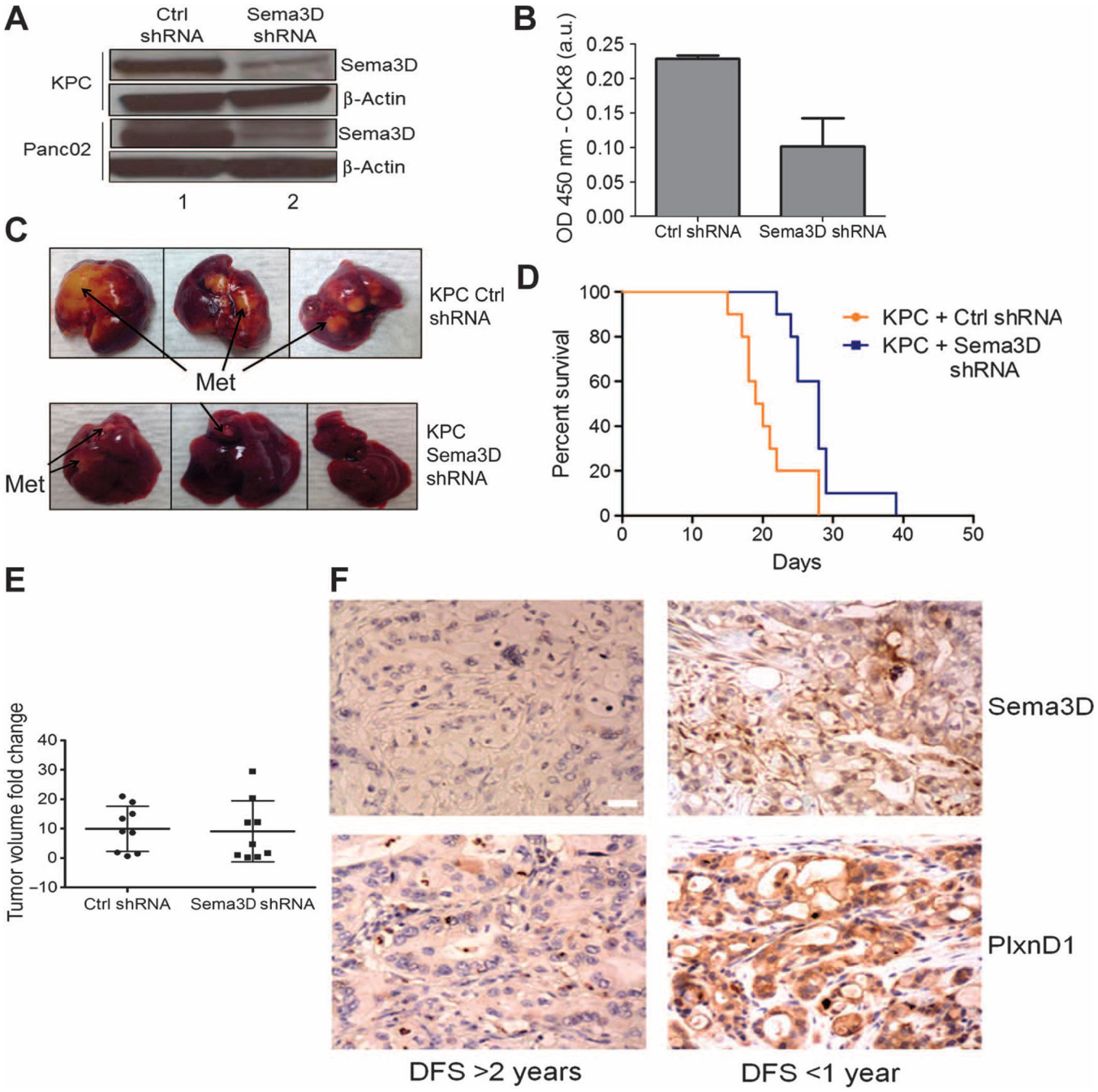

Fig. 5. Sema3D is involved in invasion and metastasis of PDA and is associated with poor survival

(**A**) Western blot confirming *SEMA3D* knockdown by shRNA. Blots are representative of at least two experiments. (**B**) In vitro invasion assay using Panc02 cells transfected with control or *SEMA3D* shRNA ($P = 0.036$, unpaired t test). Data are means ± SEM from three independent biological replicates. (**C**) Metastasis formation was assessed at day 14 in the livers from mice receiving a hemi-spleen injection of either KPC Ctrl shRNA cells (n =12 mice) or KPC *SEMA3D* shRNA cells (n =13 mice) ($P = 0.011$, Fisher's exact test). Images are representative of at least 12 mice. (**D**) Kaplan-Meier analysis of mice receiving a hemi-

spleen injection of KPC Ctrl shRNA or KPC *SEMA3D* shRNA cells (n = 10 mice per group) (P = 0.004, log-rank test). (**E**) Ultrasound was used on days 6 and 20 to assess tumor growth after implantation of subcutaneously grown KPC tumors expressing nontargeting (Ctrl) shRNA or *SEMA3D*-targeting shRNA into the pancreas of syngeneic mice. Data are presented as the tumor volumes on day 20 normalized to the tumor volumes on day 6 (n = 9 mice per group) (P = 0.84, unpaired t test). (**F**) Representative immunohistochemistry staining of PDAs from a patient with a DFS of >2 years (of 20 patients) and a patient with a DFS <1 year (of 15 patients) (P = 0.007, Fisher's exact test). Scale bar, 20 μm. Images are representative of 35 surgically resected human PDAs.

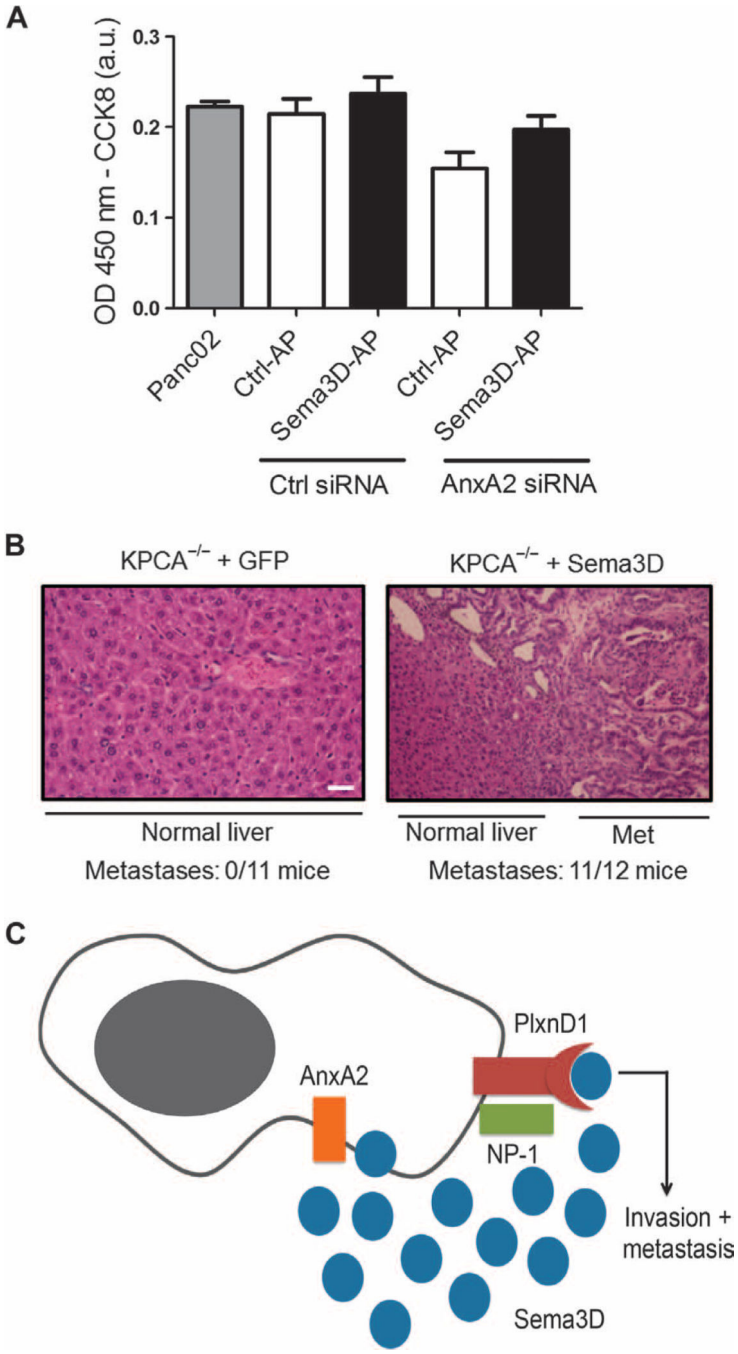

Fig. 6. Overexpression of *SEMA3D* reverses the defect in invasion and metastasis formation in *ANXA2*-deficient PDA cells

(**A**) The invasion potential of Panc02 cells was assessed after siRNA knockdown of *ANXA2* expression ($P = 0.029$, Ctrl-AP and Ctrl siRNA versus Ctrl-AP and *ANXA2* siRNA; unpaired *t* test), as well as after siRNA knockdown of *ANXA2* and overexpression of *SEMA3D-AP* ($P = 0.1205$, Ctrl-AP and *ANXA2* siRNA versus Sema3D-AP and *ANXA2* siRNA; unpaired *t* test). CCK8 was used to quantify the number of invaded cells. Data are means ± SEM from four independent biological replicates. (**B**) Representative H&E staining

of livers from mice receiving a hemi-spleen injection of either KPCA$^{-/-}$ + *GFP* cells or KPCA$^{-/-}$ + SEMA3D cells (n = 12 mice) ($P < 0.001$, Fisher's exact test). Scale bars, 20 μm. Images are representative of at least 11 mice. (**C**) Model showing the proposed interaction between AnxA2, Sema3D, and PlxnD1 in PDA cells. AnxA2 regulates the secretion of Sema3D from PDA cells, allowing it to interact with its receptor, PlxnD1. Invasion and metastasis is induced after Sema3D binding to PlxnD1 on the surface of the PDA cell.

Table 1

Functional assignment of gene expression changes in *KPCA*$^{-/-}$ mice

The number of genes in each subset of functional categories that are increased or decreased in abundance in KPC versus KPCA$^{-/-}$ primary pancreatic tumor cell lines.

	No. of genes with fold change >1.5/total genes in the set*		No. of genes with fold change >1.5/total genes in the set*
Cell movement	54/433	Cell morphology and remodeling	8/22
	46/277		20/97
			15/68
TGF-β pathway	55/394	Adhesion	14/58
			17/77
Signaling	39/293	Cell movement	55/433
	47/369		43/277
		Cell cycle	23/112
Differentiation and development	10/36	TGF-β pathway	32/394
	44/281		
		Signaling	49/293
			26/166

Asterisk denotes that if more than two gene sets in the same functional categories were identified, the two gene sets with the most significant *P* values are shown here.

Table 2

Metastasis formation in mice after orthotopic implantation of either KPC tumor cells with control shRNA or KPC tumor cells with Sema3D shRNA

$P = 0.006$, Fisher's exact test.

shRNA in KPC tumor cells	No. of mice with metastases
Control shRNA ($n = 10$ mice)	9
SEMA3D shRNA ($n = 9$ mice)	2

Table 3
Sema3D positivity in patient primary and metastatic tumors

The percentage of patients with Sema3D present in their primary tumors and metastatic sites by disease status at their time of death.

Disease status at the time of death	Local disease or oligometastatic disease	Widely metastatic disease	
Percentage of patients whose primary tumors produce Sema3D	23.1% (3 of 22 patients)	63.6% (14 of 22 patients)	
		Primary tumor	Metastatic site
Percentage of primary tumors or metastatic sites producing Sema3D in patients who died with widely metastatic disease		63.6% (14 of 22)	77.3% (17 of 22)